© 2021. Published by The Company of Biologists Ltd | Journal of Cell Science (2021) 134, jcs258391. doi:10.1242/jcs.258391

RESEARCH ARTICLE

Importin-9 regulates chromosome segregation and packaging in *Drosophila* germ cells

Victor Palacios[1], Garrett C. Kimble[2], Tina L. Tootle[2] and Michael Buszczak[1,3,*]

ABSTRACT

Germ cells undergo distinct nuclear processes as they differentiate into gametes. Although these events must be coordinated to ensure proper maturation, the stage-specific transport of proteins in and out of germ cell nuclei remains incompletely understood. Our efforts to genetically characterize *Drosophila* genes that exhibit enriched expression in germ cells led to the finding that loss of the highly conserved Importin β/karyopherin family member Importin-9 (Ipo9, herein referring to Ranbp9) results in female and male sterility. Immunofluorescence and fluorescent *in situ* hybridization revealed that *Ipo9*^{KO} mutants display chromosome condensation and segregation defects during meiosis. In addition, *Ipo9*^{KO} mutant males form abnormally structured sperm and fail to properly exchange histones for protamines. Ipo9 physically interacts with proteasome proteins, and *Ipo9* mutant males exhibit disruption of the nuclear localization of several proteasome components. Thus, Ipo9 coordinates the nuclear import of functionally related factors necessary for the completion of gametogenesis.

This article has an associated First Person interview with the first author of the paper.

KEY WORDS: Nuclear import, Karyopherin, Meiosis, Chromatin, Chromosome condensation, Nuclear actin, Histone, Protamine

INTRODUCTION

Subcellular compartmentalization allows for complex modes of gene regulation in eukaryotic cells. The regulated and active transport of macromolecules between different compartments promotes cellular homeostasis and often drives differentiation. Transport of molecules from the cytoplasm to the nucleus depends on a family of proteins called karyopherins, also known as importins (Chook and Blobel, 2001; Çağatay and Chook, 2018). The karyopherin superfamily of transporters consists of importin α and importin β subgroups. All the proteins within this karyopherin superfamily share tandem huntingtin, elongation factor 3, protein phosphatase 2A and mechanistic target of rapamycin (HEAT) repeats. These repeats allow these proteins to bind to various cargo proteins, which often, but not always, contain a nuclear localization signal within their peptide sequence. Karyopherins then transport these cargoes into the nucleus through nuclear pores.

[1]Department of Molecular Biology, University of Texas Southwestern Medical Center, Dallas, TX 75390, USA. [2]Department of Anatomy and Cell Biology, University of Iowa Carver College of Medicine, Iowa City, IA 52242, USA. [3]Center for Regenerative Science and Medicine, University of Texas Southwestern Medical Center, Dallas, TX 75390, USA.

*Author for correspondence (michael.buszczak@utsouthwestern.edu)

M.B., 0000-0001-6361-3654

Handling Editor: David Glover
Received 8 January 2021; Accepted 10 February 2021

Another key component of the transport machinery is the small GTPase Ran (Cautain et al., 2015). Cytoplasmic Ran is typically maintained in a GDP-bound state, whereas nuclear Ran binds GTP. This concentration gradient of GDP and GTP bound Ran provides a directional cue for the transport of proteins between the cytoplasm and nucleus. Once importins enter the nucleus, high affinity interactions with RanGTP cause karyopherins to release their cargoes and recycle back to the cytoplasm.

Accumulating evidence suggests that β-karyopherins do not simply function as constitutive and redundant housekeeping proteins. Interactions between different β-karyopherins with specific cargoes depend not only on their overlapping expression patterns in time and space, but also on clear differences in the affinities of the physical interactions (Plafker and Macara, 2002; Quan et al., 2008; Gontan et al., 2009; Major et al., 2011; Kimura and Imamoto, 2014). For example, histones can bind to multiple β-karyopherins, but their affinities vary. For example, Kapβ2 and Imp5 exhibit very strong affinity for Histone H3, whereas Impβ, Imp4, Imp7, Imp9 and Impα display weaker interactions (Soniat et al., 2016). Additionally, a previous study identified a group of 468 cargoes for 12 β-karyopherins (Kimura et al., 2017). Three hundred and thirty two of these cargoes were unique to one β-karyopherin family member, suggesting a division of function among these transporters. Several β-karyopherin family members have been associated with specific diseases. Accumulating evidence shows that β-karyopherins are overexpressed in multiple tumors including melanoma, pancreatic, breast, colon, gastric, prostate, esophageal, lung cancer and lymphomas (Turner et al., 2012; Fujii et al., 2018). Additionally, specific karyopherin-β proteins, such as exportin-1, have been implicated in drug resistance in cancer (Turner et al., 2012, 2014; Mahipal and Malafa, 2016).

Many importins exhibit enriched expression in gonads and are functionally required during different stages of spermatogenesis and oogenesis across many species, including *Drosophila*. *Drosophila* ovaries are organized into discrete units called ovarioles, which contain a series of sequentially developing egg chambers. Each egg chamber is comprised of 16 germ cells, 15 nurse cells and one oocyte, surrounded by a layer of somatic follicle cells. The initiation of meiosis occurs early in oogenesis, marked by the formation of the synaptonemal complex (SC) and the generation of the programmed double strand breaks. After these first events, oocytes remain arrested in prophase 1 of meiosis until stage 12, followed by prometaphase 1 at stage 13 and metaphase 1 at stage 14 (Hughes et al., 2018).

The *Drosophila* testis is structured as a closed-end coiled tube. At the tip of the testis, 10-14 germline stem cells (GSCs) surround a small cluster of somatic cells called the hub. GSCs typically divide asymmetrically to produce another GSC and a gonialblast. Gonialblasts become enveloped by two somatic cyst cells, which function in an analogous manner to the Sertoli cells of the mammalian testis (White-Cooper, 2010). The *Drosophila* gonialblast goes through four incomplete mitotic divisions to form an interconnected 16-cell spermatogonial cell cyst. Each

Journal of Cell Science (2021) 134, jcs258391. doi:10.1242/jcs.258391

spermatocyte within the cyst undergoes meiosis, resulting in the formation of cysts that contain 64 interconnected haploid cells. Immediately after the completion of meiosis, these cells enter the 'onion stage', which is marked by the appearance of the nebenkern, a two-stranded helical structure derived from mitochondria. Defects in meiosis can result in the appearance of fragmented nebenkern and alterations in the normal 1:1 ratio of nuclei and nebenkerne.

Spermiogenesis is marked by nuclear elongation and chromatin reorganization. Nuclear elongation is dependent on microtubules from the basal body that associate with the nucleus (Fabian and Brill, 2012). Chromatin organization switches from a histone-based to protamine-based packaging in the late elongation stage (Rathke et al., 2007). During elongation, the nuclear envelope that is in contact with the basal body forms a cavity that fills with microtubules while the nucleus takes on a 'canoe' shape. During chromatin reorganization, histones are ubiquitylated by an unknown ubiquitin ligase and subsequently degraded by the proteasome at the late canoe stage, immediately before protamines are incorporated into the chromatin (Zhong and Belote, 2007; Awe and Renkawitz-Pohl, 2010). After histone removal, the transition like-protein (Tpl) is incorporated, which facilitates protamine incorporation (Rathke et al., 2007). In *Drosophila*, mature sperm contain Mst35Ba (protamine A), Mst35Bb (protamine B) and Mst77F (Rathke et al., 2010). Towards the end of spermiogenesis, sperm form their own membranes in a process called individualization (Fabian and Brill, 2012).

In *Drosophila*, mutants in several importins develop normally into adults, but exhibit various defects in fertility. Importin α2 mutant males exhibit a dramatic decrease in the formation of individualized and motile sperm, whereas mutant females produce small and deflated eggs with missing or fused dorsal appendages (Giarrè et al., 2002; Mason et al., 2002). Similarly, mutations in Importin α1 also cause male and female sterility, marked by egg-laying defects in females and the formation of spermatocytes with abnormally large round nuclei in males, and loss of Importin α3 leads to the arrest of oogenesis (Máthé et al., 2000). The specific cargoes responsible for these phenotypes remain unknown.

Here, we report that null mutations in *Ipo9* (also known as *Ranbp9*) cause disruption of chromosome segregation and condensation during meiosis in both female and male *Drosophila*. Previous results have shown that Ipo9 helps to traffic Actin, Histone H2A-H2B dimers and a variety of other factors into nuclei (Kortvely et al., 2005; Dopie et al., 2012; Matsumiya et al., 2013; Sokolova et al., 2018; Padavannil et al., 2019). We confirm that loss of *Drosophila* Ipo9 disrupts the accumulation of nuclear actin during oogenesis. In addition, we find Ipo9 promotes chromosome segregation during meiosis, and the exchange of histones for protamines during spermiogenesis. Biochemical experiments suggest that Ipo9 physically associates with proteasome components, and immunofluorescence studies show that loss of Ipo9 disrupts the normal trafficking of the proteasome into germ cell nuclei during spermiogenesis. Together, these data reveal new processes directly regulated by a specific nuclear transport factor during gametogenesis.

RESULTS

Loss of Importin-9 results in sterility

We sought to genetically characterize genes that display enriched transcription within gonads based on publicly available modEncode RNA-seq data. According to these datasets, the Importin β/karyopherin family member Ranbp9 (CG5252) exhibits high levels of expression in both ovaries and testes relative to other tissues (http://flybase.org/reports/FBgn0037894). The name Ranbp9 has previously been used for genes that do not share extensive homology with one another across species. For example, the mammalian Ranbp9 gene shares closest homology to the *Drosophila* RanBPM gene, whereas mammalian Importin-9 (Ipo9) represents the closest homolog of *Drosophila* CG5252. Given these discrepancies, we have elected to call CG5252 Importin-9 (Ipo9) hereafter.

To determine whether Ipo9 functions during germ cell development in both females and males, we generated a molecular null mutation by replacing most of the Ipo9 coding sequence with a 3XP3-DsRed cassette using CRISPR/Cas9-mediated genomic engineering (Fig. S1A). Independent isolates of this $Ipo9^{KO}$ mutation were homozygous viable but exhibited female and male sterility. $Ipo9^{KO}$ homozygous

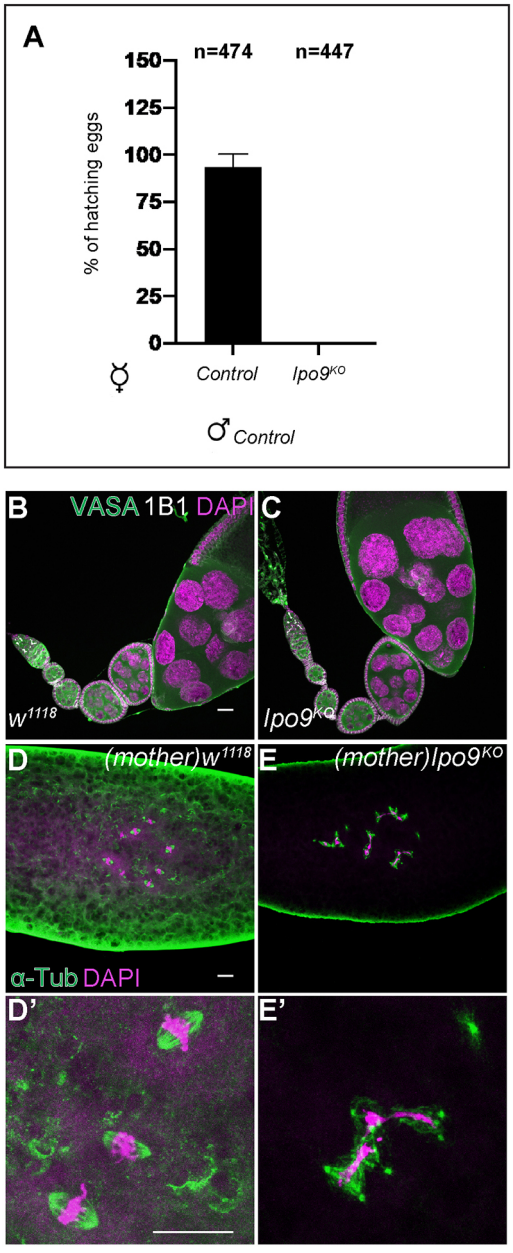

Fig. 1. Embryos from $Ipo9^{KO}$ females show mitotic defects. (A) Percentage of eggs that hatch 5 days after being laid by w^{1118} or $Ipo9^{KO}$ females crossed with w^{1118} males. (B,C) *Drosophila* ovarioles stained for VASA (green), 1B1 (white) and DAPI (magenta). w^{1118} control (B) and $Ipo9^{KO}$ ovarioles (C). (D,D′) Embryos from w^{1118} (control) and (E-E′) $Ipo9^{KO}$ females stained for α-Tub (green) and DAPI (magenta). Data are mean±s.d. Scale bars: 20 µm.

Journal of Cell Science (2021) 134, jcs258391. doi:10.1242/jcs.258391

females laid a comparable number of the eggs to w^{1118} controls and their ovaries appeared grossly normal (Fig. 1A-C). However, none of the eggs from the *Ipo9* mutants hatched. Staining for α-Tubulin and DNA revealed that loss of maternal *Ipo9* results in widespread mitotic catastrophes during the earliest embryonic divisions, marked by chromosome bridges, chromosome fragmentation, lack of chromosome condensation and an array of spindle defects (Fig. 1D-E′).

The N-terminal β-karyopherin domain is necessary for Importin-9 function

To verify that the female sterility of $Ipo9^{KO}$ homozygotes was caused by loss of *Ipo9*, and not disruption of another nearby gene, we used two methods: RNAi knockdown and cDNA rescue. Driving *Ipo9*-specific RNAi using germ cell-specific drivers resulted in the same female sterile phenotypes as the $Ipo9^{KO}$ mutant (Fig. S1C-E). This result supports the idea that Ipo9 functions during gametogenesis. Moreover, these data indicate that *Ipo9* acts in a cell-autonomous manner within germ cells to promote fertility.

To complement the RNAi knockdown experiments, we also attempted to rescue the $Ipo9^{KO}$ mutant with a full-length wild-type cDNA transgene (*UASp-Ipo9*^{FL}). We made a second transgene (*UASp-Ipo9*$^{\Delta N}$), in which the N-terminal β-karyopherin domain was deleted (Fig. 2A). This construct allowed us to test whether the *Ipo9* mutant phenotypes were caused by disruption of nuclear import of

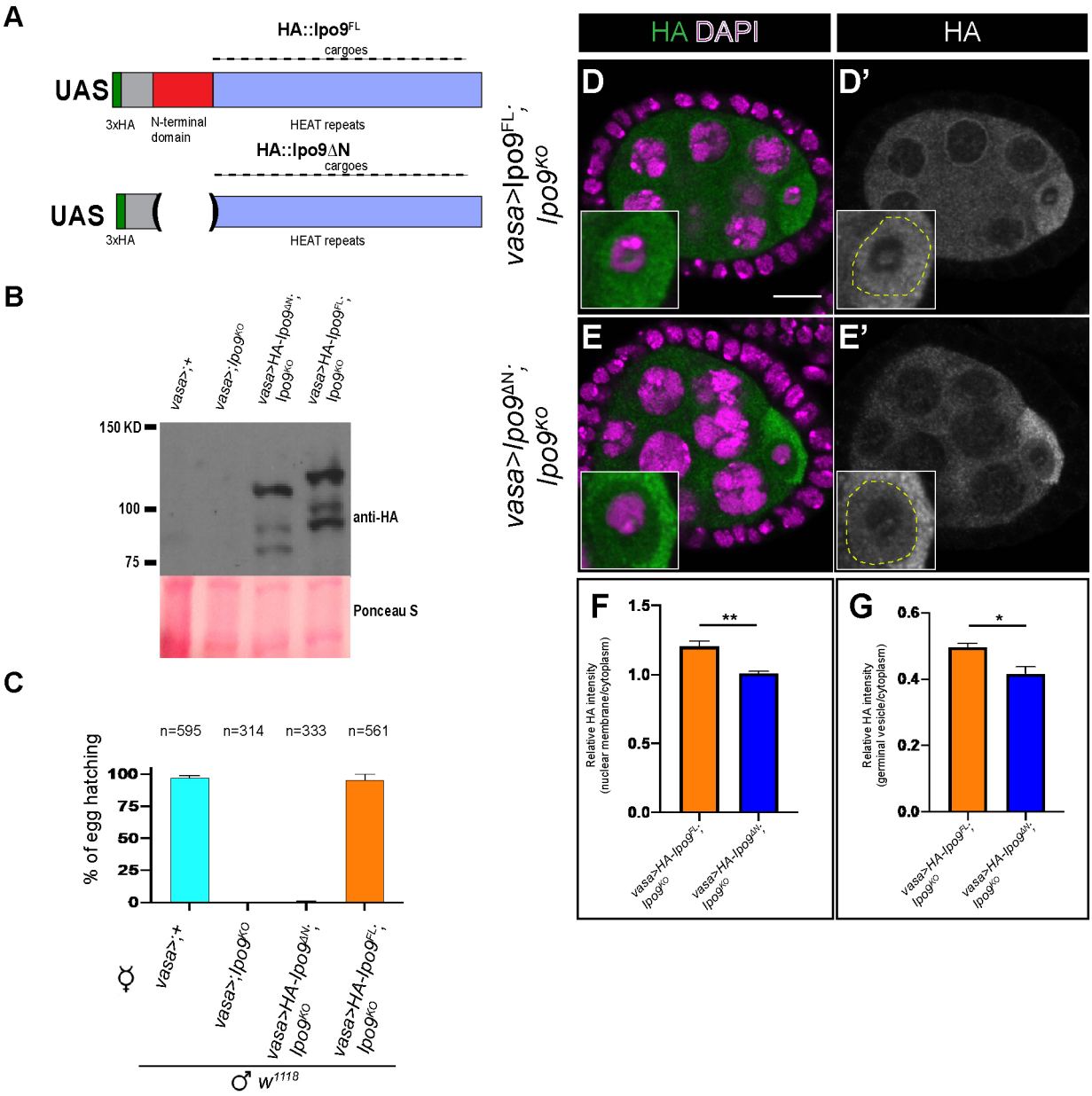

Fig. 2. The N-terminal domain of Ipo9 is required for its function during gametogenesis. (A) Schematic of the 3xHA full-length Ipo9 (Ipo9^{FL}) and 3xHA DeltaN-Ipo9 (Ipo9$^{\Delta N}$) proteins. (B) Western blot from ovaries showing HA::Ipo9$^{\Delta N}$ and HA::Ipo9^{FL} expression. (C) Percentage of eggs that hatch 5 days after being laid by *vasa-gal4>;+*, *vasa-gal4>;Ipo9*^{KO}, *vasa-gal4>Ipo9*$^{\Delta N}$*;Ipo9*^{KO} and *vasa-gal4>Ipo9*^{FL}*;Ipo9*^{KO} females crossed with w^{1118} males. (D-E′) Stage 4 to 5 egg chambers stained for HA (green and grayscale) and DAPI (magenta) for *vasa-gal4>Ipo9*^{FL} *;Ipo9*^{KO} (D,D′) and *vasa-gal4>Ipo9*$^{\Delta N}$*;Ipo9*^{KO} (E,E′) females. (F) The ratio of fluorescence intensity of HA-Ipo9 staining at the nuclear envelop versus in the cytoplasm of the nurse cells (n=30 for each genotype). (G) Ratio of fluorescence intensity of HA-Ipo9 staining at the germinal vesicle versus the cytoplasm of the oocyte (n=30 for each genotype). Data are mean±s.d. *P<0.05, **P≤0.01 (paired two-tailed Student's t-test). Scale bar: 10 µm.

Journal of Cell Science (2021) 134, jcs258391. doi:10.1242/jcs.258391

specific cargoes, as opposed to potential transport-independent functions. Both transgenes were expressed at similar levels but exhibited different rescuing activity and localization (Fig. 2B-E′). Although the Ipo9^{FL} HA-tagged transgenic protein was enriched around the nuclear envelop of nurse cells and appeared to enter the germinal vesicle within the oocyte, as expected, the Ipo9$^{\Delta N}$ protein did not, indicating that removal of this domain disrupted the ability of this protein to act as a nuclear importer (Fig. 2D-G). Driving the expression of the full-length transgene using *vasa-gal4* rescued the female sterile phenotypes, whereas the *Ipo9*$^{\Delta N}$ construct did not (Fig. 2C). Together, these results indicate that Ipo9-mediated nuclear trafficking is essential for normal oogenesis in *Drosophila*.

Loss of Ipo9 disrupts meiosis in females

Given that disruption of *Ipo9* leads to sterility in both females and males, we suspected that Ipo9 may play a role in meiosis. To characterize potential meiotic defects in *Ipo9* mutant females, we employed fluorescent *in situ* hybridization (FISH) using probes for the 359-bp repeat sequences near the X-chromosome centromere and the AACAC$_{(n)}$ microsatellite repeats on the second chromosome. In wild-type females, stage 14 oocytes are arrested in metaphase phase I until ovulation and the chromatin of these oocytes appears as a single mass. FISH revealed that X-chromosome and second-chromosome pairs normally orient towards opposite poles (Fig. 3A). However, *Ipo9* mutant oocytes tended to display misorientation of these chromosomes (Fig. 3B-D). This phenotype was marked by the appearance of individual X-chromosome and second-chromosome spots in the middle of the nucleus or misorientation of all the chromosomes to one side of the nucleus, indicating that loss of *Ipo9* disrupts normal chromosome segregation patterns during meiosis. Examining Centrosome identifier (CID), a centromere-specific histone H3 variant, in control and mutant meiotic nuclei provided additional evidence that loss of *Ipo9* results in chromosome misorientation during meiosis (Fig. 3E-H). These defects were not correlated with disruption of the meiotic spindle, which appears largely normal in *Ipo9* mutant cells (Fig. 3I-J′).

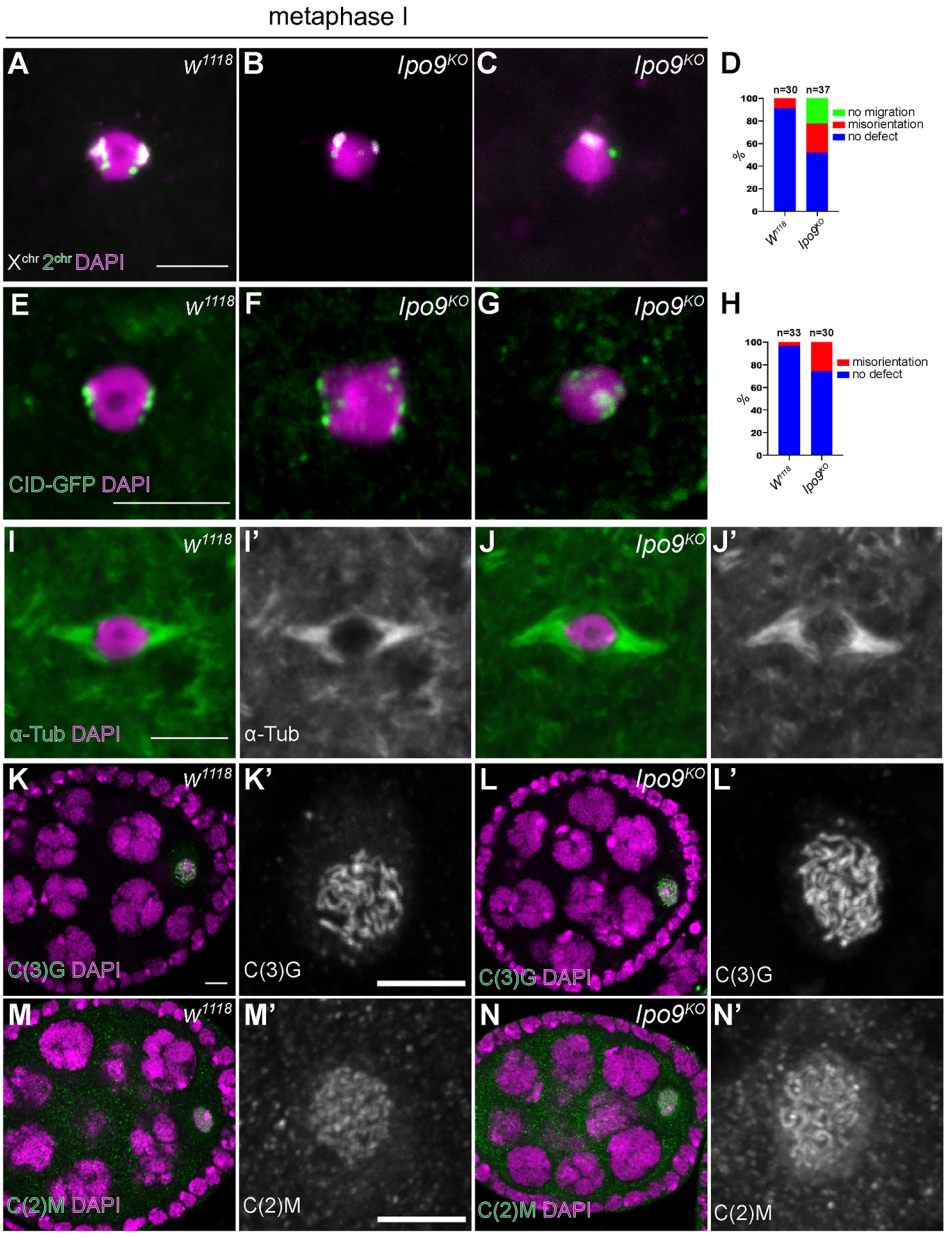

Fig. 3. *Ipo9*^{KO} oocytes at metaphase I show defects in chromosome orientation. (A-C) FISH using an X-chromosome probe (white) and second-chromosome probe (green) on oocytes in metaphase I (DAPI, magenta). (A) *w*^{1118} (A) and *Ipo9*^{KO} oocyte (B,C). (D,H) Quantification of percentage of oocytes showing chromosome orientation defects. (E-G) Control (E) and *Ipo9*^{KO} (F,G) oocytes at metaphase I stained for CID-GFP (green) and DAPI (magenta). (I-J′) Oocytes [*w*^{1118} (I-I′) and *Ipo9*^{KO} (J-J′)] at metaphase I stained for α-Tub (green) and DAPI (magenta). (K-L′) Oocytes [*w*^{1118} (K-K′) and *Ipo9*^{KO} (L-L′)] stained for C(3)G (green) at stage 4 during oogenesis. (M-N′) Oocytes [*w*^{1118} (M-M′) or *Ipo9*^{KO} (N-N′)] stained for C(2)M (green). Scale bars: 5 µm.

Journal of Cell Science (2021) 134, jcs258391. doi:10.1242/jcs.258391

Given the chromosome segregation defects we observed in *Ipo9* mutant female germ cells, we examined whether the nuclear import of meiotic specific machinery involved in sister chromosome pairing and DNA condensation was disrupted in the absence of *Ipo9*. Staining for the SC proteins, C(3)G and C(2)M, did not reveal any obvious differences between control and $Ipo9^{KO}$ ovarioles (Fig. 3K-N′). We found that loss of *Ipo9* resulted in defects in nuclear actin accumulation (Fig. S2) (Dopie et al., 2012; Belin et al., 2015; Kelpsch et al., 2016; Sokolova et al., 2018; Wineland et al., 2018). Determining the extent to which decreased levels of nuclear actin directly affect chromosome segregation or other aspects of meiosis represents important work for the future.

Loss of Ipo9 causes male sterility

Similar to the phenotypes observed in females, no progeny were produced from matings between control females and *Ipo9* mutant males (Fig. 4A). During spermiogenesis germ cell nuclei undergo dramatic shape changes to form needle-like structures. Close examination revealed that loss of *Ipo9* resulted in a failure of spermatid nuclei to change shape during spermiogenesis (Fig. 4B-E). The clustered post-meiotic mutant nuclei remained round well beyond the stage during which they should have initiated changes in nuclear shape, resulting in the absence of mature sperm. We also compared sperm tail elongation and sperm individualization between control and $Ipo9^{KO}$ testes. Staining for α-Tubulin (α-Tub) to label the sperm tails did not reveal obvious differences between w^{1118} and $Ipo9^{KO}$ testes (Fig. S3A-B′). However, staining control and mutant testes using fluorescently labeled phalloidin (Cagan, 2003; Fabian and Brill, 2012), revealed that $Ipo9^{KO}$ testes do not form actin cones or waste bags (Fig. S3C-F′ and data not shown), indicating that $Ipo9^{KO}$ spermatids do not go through individualization.

We used both RNAi knockdown and cDNA rescue as independent methods to test whether the male phenotypes were caused specifically by loss of *Ipo9*. Driving *Ipo9*-specific RNAi using germ cell-specific drivers resulted in the same phenotypes in the testis as the $Ipo9^{KO}$ mutant (Fig. S3G-I), supporting the idea that Ipo9 functions during male gametogenesis. Driving the full-length *Ipo9* cDNA transgene in an *Ipo9* mutant background using *vasa-gal4* rescued many of the morphological defects we observed during spermatogenesis, including sperm head elongation, but the $Ipo9^{\Delta N}$ transgene did not (Fig. S3J-M and data not shown). However, expression of the $Ipo9^{FL}$ transgene did not fully rescue the male sterile phenotype. Given the similarities between the $Ipo9^{KO}$ and RNAi induced phenotypes, we expect that the inability of the full-length transgene to fully rescue the male sterile phenotype is caused by the failure of *vasa-gal4*-driven *Ipo9* expression to completely recapitulate the late-stage endogenous expression pattern of the protein during spermatogenesis.

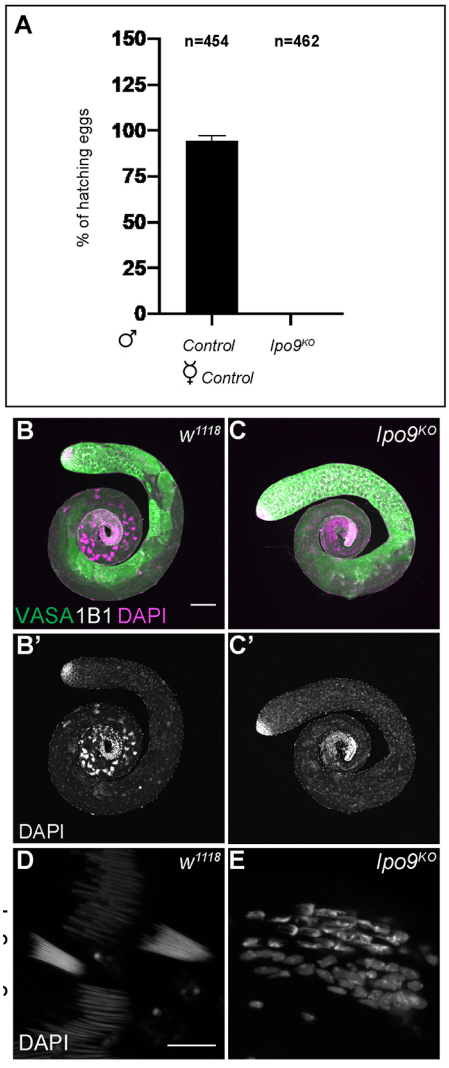

Fig. 4. $Ipo9^{KO}$ males are unable to produce mature sperm. (A) Percentage of eggs that hatch 5 days after being laid by w^{1118} females crossed with w^{1118} (control) or $Ipo9^{KO}$ males. (B-C′) *Drosophila* testes [w^{1118} (control) (B-B′) and $Ipo9^{KO}$ (C-C′)] stained for VASA (green), 1B1 (white) and DAPI (magenta). (D,E) Cluster of elongating spermatids stained with DAPI [w^{1118} (D) and $Ipo9^{KO}$ (E) testes]. Data are mean±s.d. Scale bars: 100 µm (B-C′); 10 µm (D,E).

Ipo9 functions during male meiosis

To begin to characterize whether male germ cells exhibit meiotic defects similar to what we observe in females, we crossed a GFP-tagged mitochondrial marker into the *Ipo9* mutant background so that we could examine the morphology of the nebenkern immediately after the completion of meiosis II (White-Cooper, 2004). Co-labeling for the mitochondrial marker and DNA showed that *Ipo9* mutants often exhibited defects at the onion stage, marked by the appearance of variably sized nuclei and nebenkerne (Fig. 5A-D). In addition, the chromatin of *Ipo9* mutant nuclei appeared less condensed than control nuclei at the same stage of development (Fig. 5A″-D).

Next, we performed FISH experiments on wild-type and *Ipo9* mutant testes using probes specific for the X and Y chromosomes, focusing on the onion stage, just after the completion of meiosis II. As expected, half of the round spermatids in control samples were labeled with the probe for the X chromosome, whereas the other half carried a Y chromosome. By contrast, chromosome segregation defects were apparent in *Ipo9* mutant meiotic nuclei. We observed that 40% of *Ipo9* mutant spermatids contained neither an X nor a Y chromosome, both the X and Y chromosome, two X chromosomes or two Y chromosomes at a stage when meiosis II should have been completed (Fig. 5E-J). These results indicate that loss of *Ipo9* disrupts normal meiosis, at least in some fraction of male germ cells.

Loss of *Ipo9* disrupts histone to protamine exchange in testes

As noted in our initial phenotypic characterization, *Ipo9* mutant spermatid nuclei remained round and failed to undergo the normal morphological changes that occur during the process of nuclear shaping. Shape changes in developing sperm occur as histones are being exchanged for protamines, but whether direct links between

Journal of Cell Science (2021) 134, jcs258391. doi:10.1242/jcs.258391

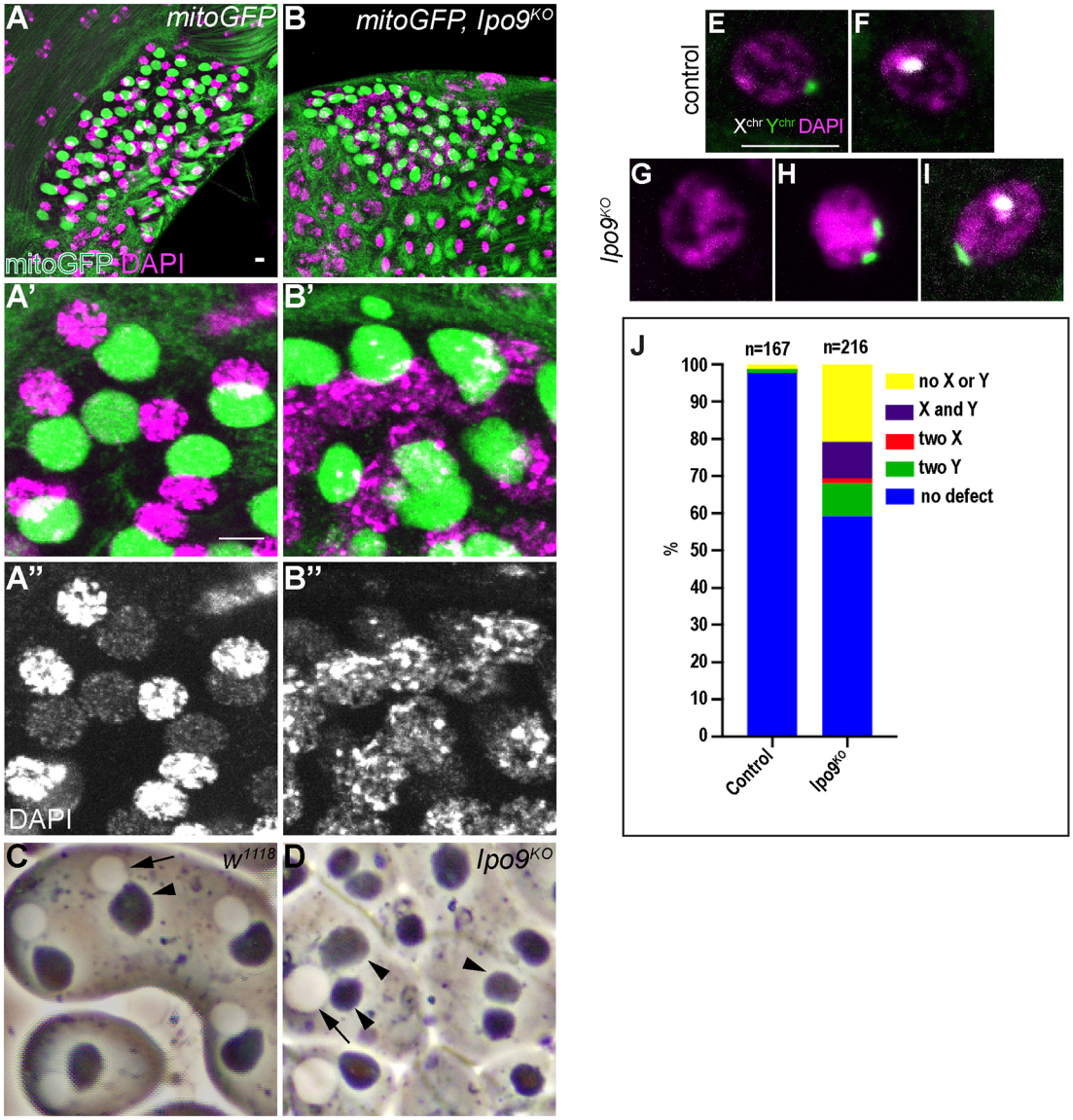

Fig. 5. *Ipo9*^{KO} spermatids exhibit chromosome segregation defects. (A,B) Spermatids at the onion stage stained for GFP (green) and DAPI (red). (A-A″) Control shows a 1:1 ratio of condensed nuclei and rounded nebenkern. (B-B″) *Ipo9*^{KO} mutants exhibit nebenkern number and size defects. *Ipo9* mutant germ cells also display DNA condensation defects. (C,D) Phase contrast images of testes from *w*^{1118} control (C) and *Ipo9*^{KO} males (D). Arrows point to nuclei and arrowheads point to nebenkern. (E-I) FISH using an X-chromosome probe (white), Y-chromosome probe (green) and DAPI (magenta) on spermatids at the onion stage [control (E,F) and *Ipo9*^{KO} (G-I) spermatids]. (J) Quantification of the percentage of spermatids showing chromosome segregation defects. Scale bars: 5 µm.

these processes exist remains unclear (Fabian and Brill, 2012). We examined whether histones were removed properly and replaced by protamines during the final stages of sperm development. Control spermatids showed replacement of the histone H2A and H2Av at the late elongation stage by protamine-B and overlapping of histone H2A or H2Av with protamine-B was almost never observed (Fig. 6A,C-C‴; Fig. S4A). By contrast, *Ipo9*^{KO} spermatids accumulated nuclear protamine-B in the presence of histone H2A and H2Av, neither of which were completely removed from germ cell nuclei (Fig. 6B,D-D‴; Fig. S4B). Based on these results, we conclude that *Ipo9*^{KO} spermatids have a defect in the chromatin packaging switch that marks mature sperm.

The ubiquitin proteasome pathway has been implicated in histone degradation during spermiogenesis (Zhong and Belote, 2007). Because *Ipo9*^{KO} spermatids have a defect in histone removal, we decided to explore whether histone ubiquitylation is impaired in *Ipo9*^{KO} testes. Staining for polyubiquitylation in control testes showed spermatids positive for ubiquitylation (Fig. 6C-C‴). However, nuclei that were in transition to protamine incorporation or had already accumulated protamines, were negative for polyubiquitylation. Similar to control testes, *Ipo9*^{KO} testes have germ cells that were positive for ubiquitylation during early stages of sperm development (Fig. 6D-D‴). *Ipo9*^{KO} spermatid nuclei also contained low levels of ubiquitylation at later stages when they begin to accumulate high levels of protamines, suggesting that loss of Ipo9 disrupts the transition from histone to protamine-based chromatin packaging downstream of histone ubiquitylation.

Ipo9 promotes the nuclear import of proteasome components during the late stages of sperm development

In an attempt to identify potential Ipo9 cargoes for nuclear import during male germ cell development, we immunoprecipitated Ipo9

Journal of Cell Science (2021) 134, jcs258391. doi:10.1242/jcs.258391

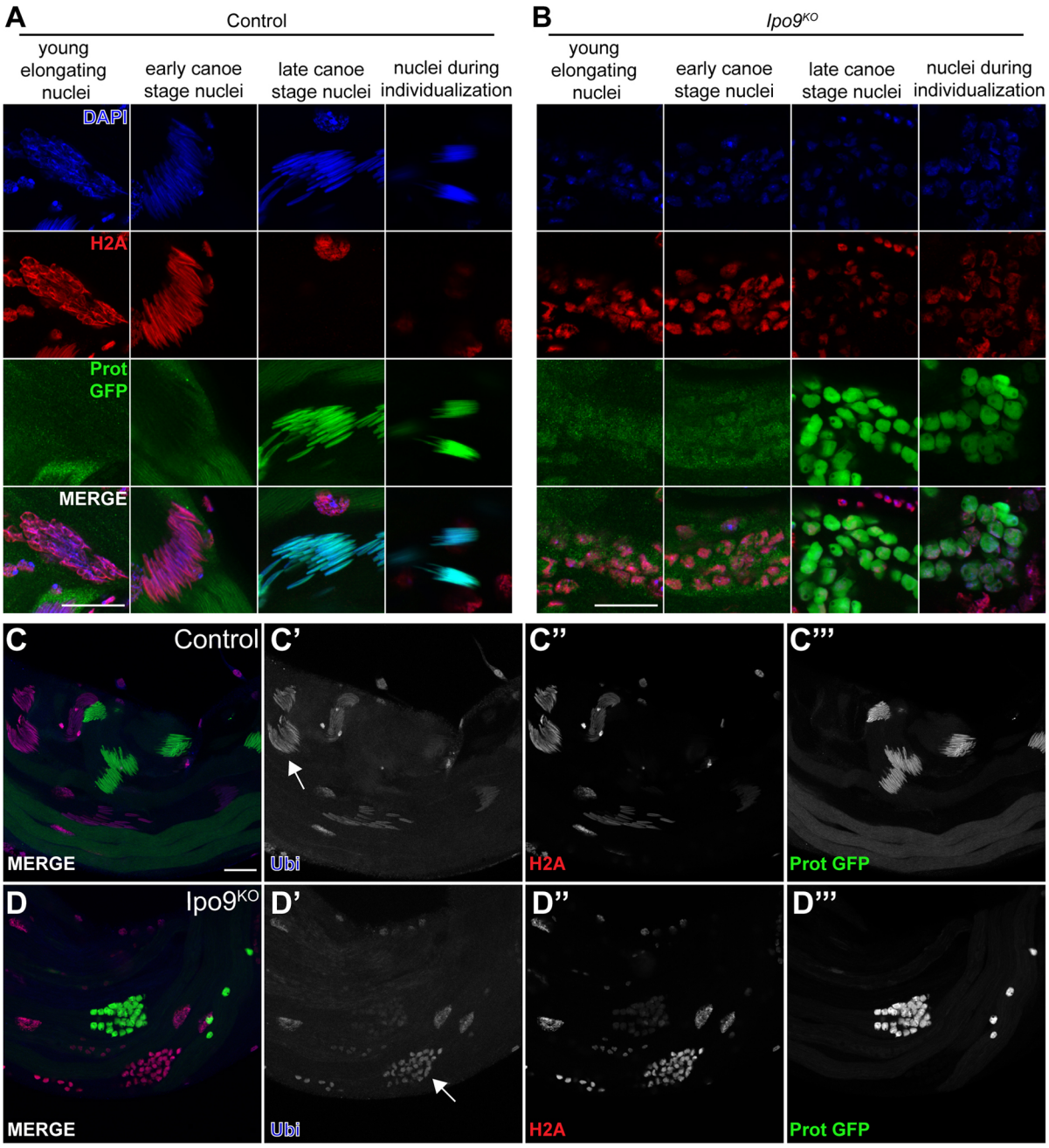

Fig. 6. *Ipo9*^{KO} spermatids show defects in H2A removal. (A,B) Elongating nuclei stained for H2A (red), ProtB-GFP (green) and DAPI (blue). (A) *w*^{1118} control nuclei are able to elongate and replace histone with protamine-B. (B) *Ipo9*^{KO} nuclei are unable to elongate and properly remove histones. (C-D‴) Testes stained for ubiquitin (blue), H2A (red) and ProtB-GFP (green). *w*^{1118} control and *Ipo9*^{KO} nuclei are positive for ubiquitylation before protamine incorporation (white arrows). Scale bars: 20 µm.

from testes using the HA-tagged rescuing transgene under control of a *vasa-gal4* driver. Mass spectrometry analysis revealed proteins that showed enrichment in the Ipo9 immunoprecipitation (IP) pellet versus the control IP pellet (Table S3). As noted above, ubiquitylation plays a central role in removing histones from chromatin during the histone to protamine exchange that occurs during spermiogenesis (Rathke et al., 2007). However, the ubiquitin ligase responsible for this activity remains unknown. Interestingly, Ipo9 appears to associate with a number of ubiquitin ligases, including CG5382, CG31642, Sinah, Hyperplastic discs and KLHL10 (Table S3), the last two of which exhibit male sterility when mutated (Mansfield et al., 1994; Arama et al., 2007; Kaplan et al., 2010).

We also noted that several components of the proteasome, including Rpn1 and Rpt1 among others, appeared to associate with Ipo9. Previous efforts to define the global interactome of *Drosophila* proteins had also noted these same physical interactions (Guruharsha et al., 2011). To determine the functional significance of these results, we examined the subcellular distribution of several proteasome proteins, for which the necessary tagged transgenes have been developed, during the late stages of sperm development. This analysis showed that loss of *Ipo9* disrupts the normal nuclear import of

Journal of Cell Science (2021) 134, jcs258391. doi:10.1242/jcs.258391

Prosα3T, Prosα6T and Prosα2. For example, wild-type germ cells at the onion stage exhibited nuclear Prosα2 with little to no cytoplasmic localization (Fig. 7A-A‴). Although *Ipo9*^{KO} germ cells also accumulated some nuclear Prosα2 during this stage, we observed robust cytoplasmic Prosα2 staining as well, suggesting that not all the Prosα2 was being trafficked to the nucleus (Fig. 7B,E). This trend continued into the early canoe stage, when nuclear shape changes begin to occur and as histones are being replaced by protamines. In

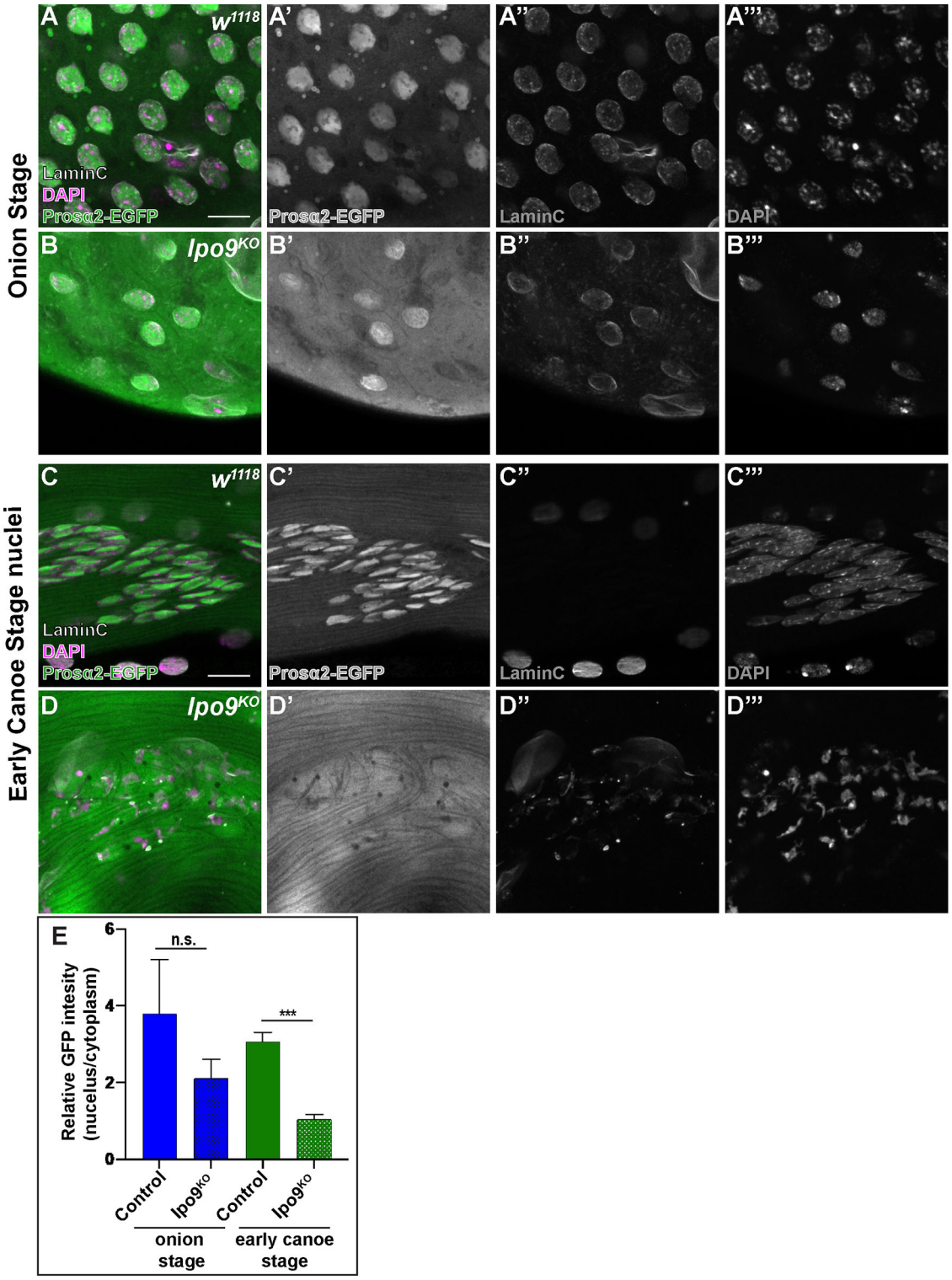

Fig. 7. *Ipo9*^{KO} spermatids show reduction of Prosα2 in the nucleus. (A-D) Spermatids [w^{1118} (A,C) and *Ipo9*^{KO} (B,D)] at the onion stage and early canoe stage, stained for Prosα2-EGFP (green), LaminC (white) and DNA (DAPI; magenta). (E) Quantification of relative fluorescence intensity of Prosa2-EGFP in the nuclei and cytoplasm of control and *Ipo9*^{KO} samples. n=45 for each genotype at the onion stage and n=40 for each genotype at early canoe stage. Data are mean±s.d. ***$P\leq0.001$; n.s., not significant ($P>0.05$) (paired two-tailed Student's t-test). Scale bars: 10 µm.

Journal of Cell Science (2021) 134, jcs258391. doi:10.1242/jcs.258391

wild-type samples, Prosα3T, Prosα6T and Prosα2 localized to the nucleus and little of the protein remained in the cytoplasm (Fig. 7C,E; Figs S5, S6). By contrast, *Ipo9*^{KO} cells always exhibited high levels of Prosα3T, Prosα6T and Prosα2 in the cytoplasm at this stage (Fig. 7D, E; Figs S5, S6). These results indicate that Ipo9 may play a specific role in the efficient nuclear trafficking of factors that help to coordinate the chromatin re-organization that occurs late in *Drosophila* sperm development. However, biochemical experiments failed to detect robust direct physical interactions between Ipo9 protein and individually expressed Prosα3T, Prosα6T and Prosα2 (Fig. S7). Lastly, although Lamin C was completely removed from the nuclear envelop during the late stages of sperm development in control cells (Fig. 7; Figs S5, S6), we also observed residual Lamin C at the nuclear periphery in the absence of Ipo9, suggesting these mutants have additional defects in the remodeling of nuclear architecture.

DISCUSSION

Here, we provide evidence that *Ipo9* specifically regulates a number of critical processes during *Drosophila* gametogenesis. *Ipo9* null mutants survive to adulthood but exhibit female and male sterility. In the ovary, loss of *Ipo9* results in defects in chromosome orientation and segregation during meiosis, resulting in mitotic catastrophes during early embryogenesis in progeny derived from *Ipo9* homozygous mutant females. *Ipo9* mutant males also exhibit numerous phenotypes during germ cell development, including defects in meiosis, and disruption of the nuclear shape changes and failure to fully exchange histones for protamines during spermiogenesis. Together, these represent a unique spectrum of phenotypes compared to other *Drosophila* β-karyopherin family members. Of the 12 *Drosophila* β-karyopherin genes that have been genetically characterized, loss-of-function alleles in seven result in lethality (Jakel and Gorlich, 1998; Collier et al., 2000; Lippai et al., 2000; Baker et al., 2002; Tekotte et al., 2002; Ilius et al., 2007; Giagtzoglou et al., 2009; Higashi-Kovtun et al., 2010; Natalizio and Matera, 2013; Jäckel et al., 2015; Kahsai et al., 2016; VanKuren and Long, 2018). Several other importin mutants do survive until adulthood, including *ebo*^{mut}, *apl*^{null} and *arts*^{null}. *ebo*^{mut} homozygotes display neuronal defects, *apl*^{null} mutants are male sterile, whereas *arts*^{null} mutant females produce smaller eggs that cannot be fertilized (Collier et al., 2000; Ilius et al., 2007; VanKuren and Long, 2018). In addition, a *ketel* dominant negative mutant (*ketel*^{D}) shows a female sterile phenotype and embryos derived from these flies exhibit chromosome segregation defects somewhat similar to those displayed by *Ipo9*^{KO} mutants (Schupbach and Wieschaus, 1991; Tirian et al., 2000; Timinszky et al., 2002). Thus, amongst *Drosophila* karyopherin family members studied to date, *Ipo9* is the only gene that displays specific defects during meiosis in both females and males, and in late sperm development, when mutated.

Transgenic rescue experiments confirm that Ipo9 functions to promote the transport of proteins from the cytoplasm to the nucleus during oogenesis and spermatogenesis. A full-length Ipo9 transgene rescues most of the sterile phenotypes exhibited by *Ipo9* mutants when driven in the germline. We suspect the failure of the Ipo9 wild-type transgene to fully rescue the male sterility of the mutant is likely due to the failure of the *vasa-gal4* driver to fully recapitulate the endogenous expression pattern of *Ipo9*. The N-terminal domains of β-karyopherin proteins normally promote cytoplasmic-to-nuclear trafficking by contacting the nuclear pore and helping cargoes move through the nuclear pore complex. This domain also binds to RanGTP, and thus participates in the cycling of importins back-and-forth between the cytoplasm and nucleus (Chi and Adam, 1997; Kutay et al., 1997; Ström and Weis, 2001; Fried and Kutay, 2003; Bange et al., 2013). Strikingly, deletion of the N-terminal karyopherin domain renders the transgene non-functional, confirming that Ipo9 acts as an essential transport factor during gametogenesis in both males and females.

The transition from histone-based to protamine-based chromatin organization is essential for the nuclear shaping that leads to a highly compact sperm nucleus (Rathke et al., 2014). *Ipo9*^{KO} nuclei are able to incorporate protamine-B, however histone H2A and H2Av are not completely removed. These results may partially explain why *Ipo9*^{KO} nuclei do not elongate properly. Evidence that the ubiquitin proteasome pathway is involved in histone removal during spermiogenesis includes the histone ubiquitylation that occurs before protamine deposition and the delay in histone removal in proteasome mutants (Zhong and Belote, 2007; Awe and Renkawitz-Pohl, 2010). Interestingly, *Ipo9*^{KO} nuclei do not exhibit strong nuclear ubiquitylation after protamine incorporation, even though they still retain nuclear histones (Fig. 6D-D″). Additionally, we observed that *Ipo9*^{KO} spermatids showed a significant reduction in the nuclear localization of several proteasome proteins, including Prosα6T, Prosα3T and Prosα2, compared to the control spermatids. These results suggest that the ligase(s) responsible for histone ubiquitylation and components of proteasome that ultimately degrade ubiquitylated histones are potential cargoes of Ipo9. Interestingly, Ipo9 appears to physically associate with a number of specific ubiquitin ligases, including Hyperplastic discs and KLHL10, which have been implicated in the regulation of male germ cell development (Mansfield et al., 1994; Arama et al., 2007; Kaplan et al., 2010), and with several components of the proteasome. Perhaps Ipo9 has evolved to temporally coordinate the import of these functionally related proteins during late sperm development. Such specialization in nuclear import may offer an economy of scale that would not exist if the responsibility of nuclear import during this critical phase of sperm development, when the cytoplasm and nuclei of sperm are becoming highly compacted, was spread across a number of potentially redundant β-karyopherins. This type of coordination in trafficking has been proposed previously in different contexts (Bange et al., 2013). Thus, further study of Ipo9 cargoes during sperm development may reveal critical unknown factors that play roles in meiosis, chromosome compaction and segregation, and nuclear shape changes.

MATERIAL AND METHODS

Fly stocks

Fly stocks were maintained at 22–25°C on standard cornmeal-agar-yeast food, unless otherwise noted. RNAi knockdown in male flies was conducted at 29°C. The following stocks were used in this study: *w*^{1118} (BL-6326); *His2Av-mRFP1* (BL-34498); *ProtamineB-eGFP* (BL-58406); *mat-α-Tub-gal4* (BL-80361 II^{chr} and III^{chr}); *MTD-gal4* (BL-31777); UAS-*Ipo9*^{RNAi} (BL-33004); and *sqh-EYFP-Mito* (BL-7194). *UASp-HA-Ipo9*^{FL} and *UASp-HA-Ipo9*^{ΔN} were inserted into attP40(BL-25709) using phiC31 integrase (Rainbow Transgenics). *vasa-gal4* was a gift from Y. Yamashita. *Prosα6T-EGFP*, *Prosα3T-EGFP* and *Prosα2-EGFP* were gifts from Dr John Belote (Syracuse University, NY).

Cloning *Ipo9*

RNA was extracted from *w*^{1118} ovaries and made into cDNA using a SuperScript II-Strand Kit (Life Technologies). We next performed PCR using Ipo9^{FL} specific primers (forward, 5'-CACCATGTCGCTGCAATT-CCAAAACG-3′ and reverse, 5'-CTACTTCTGCTGGACCTTGCTG-3′).

To generate Ipo9$^{ΔN(36\text{-}144aa)}$, we performed PCR using the following primers: forward, 5′ CACCATGTCGCTGCAATTCCAAAACG-3′ and reverse, 5'-TTCTGTCTGCTGCAGGACTCC first, and reverse, 5'-GAGGAGCGTATCTTTGAATTGGGTTCTGTCTGCTGCAGGACTCC-

3′ second, for fragment 1; and forward, 5'-CCCAATTCAAAGATACGCTCCTC and reverse, 5'-CTACTTCTGCTGGACCTTGCTG to generate fragment 2. Then PCR splicing by overhang extension was performed to stitch fragment 1 with fragment 2. PCR products were cloned into pENTR (Life Technologies) and swapped into pPHW (*Drosophila* Gateway Vector Collection) using an LR reaction.

Generating the *Ipo9^{KO}* allele

To generate the *Ipo9^{KO}* allele, guide RNAs were designed using http://tools.flycrispr.molbio.wisc.edu/targetFinder (Guide1, 5'-CTTCGCGCTATCACATGTAGTCAA-3′/5'AAACTTGACTACATGTGATAGCGC-3′ and Guide2, 5'-CTTCGGTGGACAGAAAGTTGAGTA-3′/5'AAACTACTCAACTTTCTGTCCACC-3′) and synthesized by Integrated DNA Technologies (IDT) as 5′ unphosphorylated oligonucleotides, annealed, phosphorylated and ligated into the BbsI sites of the pU6-BbsI-chiRNA plasmid (Gratz et al., 2013). Homology arms were PCR amplified and cloned into pHD-dsRed-attP (Gratz et al., 2014) (arm1F, 5'-GCTACACCTGCATGCTCGCGTTCATGTGCAAGCGCAAGTC-3′; arm1R, 5'-GTCACACCTGCACTGCTACAACGGGCGTTTTGCAAGACTG-3′; arm2F, 5'-CGTAGCTCTTCGTATCAACTTTCTGTCCACCGTTCC-3′; arm2R, 5′-CGATGCTCTTCCGACGCGAACCGAATCGTAACTGGC-3′) (Addgene). The pHD-dsRed-attP vector was cut with the enzymes AarI and SapI. Guide RNAs and the donor vector were co-injected into nosP Cas9 attP40 embryos at the following concentrations: 250 ng/ml pHDdsRed-attP donor vector and 20 ng/ml of each of the pU6-BbsI-chiRNA plasmids containing the guide RNAs (Rainbow Transgenics).

PCR verification of *Ipo9^{KO}*

PCR verification of knock-in of the *3xP3-DsRed* cassette into the *Ipo9* locus in the *Ipo9^{KO}* was carried out using the primer pairs illustrated in Fig. S1A,B. For PCR 1, a primer corresponding to an upstream sequence of the *Ipo9* locus (Ipo9Aar1outF, 5'-CAAGCCGCAAATGATGCTGCTG-3′) and a reverse primer corresponding to the DsRed sequence (DsRedstartR, 5'-CATGAACTCCTTGATGACGTCCTC-3′) were used. For PCR 2, a forward primer corresponding to the DsRed sequence (DsRedendF, 5'-GACTACACCATCGTGGAGCAG-3′) and a primer corresponding to a downstream sequence of the *Ipo9* locus (Ipo9Sap1outR, 5'-CTTTGCCTTTGGCTCAGAGAAGC-3′) were used. For PCR 3, a primer corresponding to the end of exon 2 of Ipo9 (Exon2F, 5'-GGAACTGGGTCCAGTAGTCATAC-3′) and a primer corresponding to the beginning of exon 5 of Ipo9 (Exon5R 5'-GAGGTGGAGATTCTTGATGCAC) were used.

Immunofluorescent staining in ovaries, testes and embryos

Ovaries and testes were dissected in Grace's Medium. Ovaries and testes were fixed for 10 min with gentle rocking in 4% formaldehyde in PBS. Fixed ovaries and testes were briefly rinsed three times and permeabilized in 1× PBS plus 0.3% Triton X-100 (PBST) at room temperature for 1 h before adding primary antibody.

Drosophila embryos were stained according to Mani et al. (2014). Embryos were dechorionated in 50% bleach for 2-3 min. Then embryos were rinsed in 1× PBS two times. Embryos were fixed in 50% heptane and 50% fixative solution (3 parts fixative solution, 1.33× PBS and 67 mM EGTA:1 part 37% formaldehyde) for 10 min. After fixation, the aqueous phase (bottom) was removed and replaced with an equal volume of 100% methanol. Then the embryos were vortexed rigorously for 1-2 min. Embryos were rinsed with 100% methanol two times. Then embryos were either stored at −20°C or rehydrated. To rehydrate, embryos were washed in a series of 70% MeOH: 30% PBST, 50% MeOH: 50% PBST, 30% MeOH:70% PBST and finally 100% PBST for 20 min each. Then embryos were blocked in 5% normal goat serum for 1 h at room temperature.

Incubation with primary antibody was in 3% bovine serum albumin (BSA) in PBST at 4°C for at least for 20 h. Samples were washed three times for 20 min in PBST, incubated with secondary antibody in 3% BSA in PBST at room temperature for 3-5 h and then washed three times for 20 min each in PBST. Samples were mounted in VectaShield mounting medium with DAPI (Vector Laboratories). The following antibodies were used (dilutions noted in parentheses): mouse anti-Hts (1B1) (1:20); rat anti-VASA (1:20); mouse actin-JLA20 (1:10); mouse anti-Orb (4H8) (1:10); and mouse anti-LaminC (LC28.26) (1:10) (Developmental Studies Hybridoma Bank, IA, USA); rabbit anti-Vasa-d-260 (1:200) (Santa Cruz Biotechnology); mouse anti-actin-C4 (1:100, MAB1501, MilliporeSigma); rat anti-HA 3F10 (1:100; Roche); rabbit anti-GFP (1:1000 Molecular Probes); rat anti-α-Tub (1:100, YL1/2, Abcam); chicken anti-GFP (1:1000, Novus Biological); mouse anti-ubiquitin (1:100, P4D1, Cell Signaling Technology); rabbit anti-RFP (1:1000, Rockland); rabbit anti-H2A (1:2000, from Robert L. Glaser, Wadsworth Center, NY); rabbit anti-Osk (1:1000 from Anne Ephrussi, EMBL, Heidelberg, Germany); rabbit anti-C(3)G (1:1000, from Mary Lilly, NICHD, MD; Hong et al., 2003); rabbit anti-C(2)M (1:1000, from Kim McKim, Rutgers University, NJ); and rhodamine phalloidin (1:200, R415 300U, Invitrogen). Cy3, Cy5, FITC (Jackson Laboratories) or Alexa 488 (Molecular Probes) fluorescence-conjugated secondary antibodies were used at a 1:200 dilution. Images were taken using a Zeiss LSM800 confocal microscope with a 40× oil immersion objective (numerical aperture=1.4), using exactly the same exposure times and gain settings for control and mutant samples, and processed using ImageJ with no changes in the contrast or brightness.

Quantification of HA and GFP intensities

For HA quantification on the nuclear membrane of nurse cells relative to cytoplasm, a line was drawn from the middle of the nucleus to the cytoplasmic region. DAPI was used as a reference for the nucleus. Data points adjacent to the DAPI signal were divided by data points not adjacent to the DAPI signal. For HA quantification in the germinal vesicle relative to cytoplasm, the region within the oocyte nucleus was measured and divided by the cytoplasm signal. DAPI was used to identify the oocyte nucleus. For GFP quantification of nuclear signal relative to cytoplasm signal, the region within nuclei was measured and divided by the cytoplasmic signal. DAPI was used to identified nuclei at the onion and early canoe stages. Mean±s.d. was plotted on the graph for each genotype.

Fertility assays

Males and virgin females (3-7 days old) of the appropriate genotype were mated in mating cages with grape juice (3%) agar plates with a little bit of wet yeast. The flies were allowed to lay eggs for 12-24 h at 22-25°C.

Western blotting

For protein extraction, ovaries from fattened flies were dissected in Grace's medium, physically disrupted and extracted with sample buffer with 20% β-mercaptoethanol (BME) using a pestle followed by heating at 90°C for 10 min. Protein electrophoresis and wet transfer systems were used. After running the SDS-PAGE gel, the proteins were transferred to an Amersham Hybond ECL nitrocellulose membrane (GE Healthcare, RPN2020D). For blotting, the following primary antibodies were used in fresh PBST buffer (1× PBS with 0.1% Tween 20 and 5% Bio-Rad non-fat milk): mouse anti-ActinJLA20 (1:100) and rat anti-VASA (1:10,000) from the Developmental Studies Hybridoma Bank, mouse anti-ActinC4 (1:1000, MAB1501, MilliporeSigma), mouse anti-Flag M2 (1:10,000, Sigma-Aldrich) and mouse anti-HA (1:1000, 5B1D10, Thermo Fisher Scientific). After overnight incubation at 4°C, the membranes were washed for 20 min three times in PBST buffer without milk before incubating with secondary antibodies for 2 h at room temperature. Horseradish peroxidase-conjugated anti-mouse and anti-rat secondary antibodies (Jackson Laboratories) were used at a 1:2000 dilution. After incubation with the secondary antibody, the membranes were washed three times for 20 min each and then incubated with ECL Western Blotting Detection Reagents (GE Healthcare, RPN2106).

Oocyte preparation for analysis of meiosis I

The following protocol was adopted from Radford and McKim (2016). Females fed on wet yeast were aged for 3 to 5 days at 25°C to enrich for oocytes in metaphase. Ovaries were dissected in 1× PBS solution at room temperature. For fixation, 687.5 µl of fixation buffer (1× PBS, 150 mM sucrose) was freshly mixed with 312.5 µl 16% formaldehyde. An aliquot of 0.5 ml of this solution was added to the ovaries and incubated for 2.5 mins on a nutator. An aliquot of 0.5 ml heptane was then added to the top of the fixation solution and vortexed for 1 min. The tissue was then allowed to settle for 1 min. The fixative was removed and 1 ml of 1× PBS was added to

the sample and vortexed for 30 s. Samples were allowed to settle for 1 min before another quick wash with 1× PBS. To remove the membranes, three to four pairs of ovaries were added to a glass slide. The ovaries were then separated into individual ovarioles using forceps, and 1× PBS was added as necessary to prevent the ovarioles from drying out. A coverslip was placed on top of the ovarioles and gently 'rolled' until all membranes were removed. The samples were then subjected to immunofluorescent staining or FISH.

FISH

A protocol adapted from the Fox lab was used with oligopaints (Beliveau et al., 2012, 2014, 2015). Oocytes were prepared for examining meiosis I according to Radford and McKim (2016). Testes were dissected in Grace's medium and fixed in 4% paraformaldehyde buffered in 1× PBS for 10 min. The samples were then washed once in 1× PBS for 1 min, 1× PBS plus Tween 20 (100 µl Tween 20 for every 100 ml 1× PBS) for 1 min, 1× PBS plus Triton X-100 (250 µl Triton X-100 for every 50 ml 1× PBS) for 10 min, 1× PBS plus Tween 20 (100 µl Tween 20 for every 100 ml 1× PBS) for 1 min and finally in 0.1N HCL for 5 min. The samples were then washed three times in 2× SSC with Tween 20 (SSCT) for 2 min, once in 2× SSCT/50% formamide for 5 min and once in 2× SSCT/50% formamide at 60°C for 20 min. During the final wash, the oligopaint probe (200-300 pmol) was added to the hybridization mix [12.5 µl 2× hyb cocktail (a 2:1:2 mixture of 50% dextran sulfate solution, 20× SSC and ddH_2O), 12.5 µl formamide, 1 µl 10 mg/ml RNase], mixed by vortexing and then spun down. Samples were protected from light until needed. This mixture was added to each sample and then incubated at 78°C for 2.5 min. The samples were then incubated in a 42°C water bath overnight. The samples were washed in 2× SSCT/50% formamide at 60°C for 1 min. After this wash, the samples were moved to room temperature and washed three times in 2× SSCT/50% formamide for 10 min and three times in 0.2× SSC for 10 min. The samples were then mounted in Vectashield with DAPI. The following fluorescently labeled oligos (IDT) were used for FISH:

X, 5′-Cy3-TTTTCCAAATTTCGGTCATCAAATAATCAT-3′; Y, 5′ Alexa488-N/AATACAATACAATACATTACAATACAATAC-3′; and 2, 5′-Cy5-AACACAACACAACACAACACAACACAACAC.

Immunoprecipitation followed by mass spectrometry

Preparation of crude protein lysate from fly adult testes involved 250 pairs of testes from *Vasa-gal4>+* and *Vasa-gal4>UASp-HA-Ipo9^{FL}* flies that were dissected in cold PBS. Testes were washed twice in PBS before being lysed on ice in lysis buffer [50 mM Tris (pH 8.0), 137 mM NaCl, 1 mM EDTA, 1% Triton X-100, 10% glycerol, 10 mM NaF and protease inhibitors]. After centrifugation, the supernatants were incubated with rat anti-HA (Affinity Matrix Roche) for 3-6 h at 4°C. The beads were then quickly washed three times with lysis buffer and boiled in Laemmli sample buffer with BME. Samples were submitted to the University of Texas Southwestern proteomics core for complex mixture trypsin service.

Co-immunoprecipitation of Ipo9 and proteasome proteins

RNA was extracted from *w^{1118}* ovaries and made into cDNA using a SuperScript II-Strand Kit (Life Technologies). We next performed PCRs using the following primers: *Prosα6T*-For, 5′-CACCATGTTCCGGAATCAGTATGAC-3′; *Prosα6T*-Rev, 5′-TCAATGTGCGTCACTGCCGC-3′; *Prosα2*-For, 5′CACCATGGCTACCGAACGATACAG; *Prosα2*-Rev, 5′-TTAGGGGATGCTGGCCAAGTAG-3′; *Rpn1*-For, 5′-CACCATGACGGGCGAGACCAAGCTG-3′; *Rpn1*-Rev, 5′ CTATTTCACAAAATTTGGGTTCTTTTTCAGTATAACG-3′; *Rpn3*-For, 5′-CACCATGACCAACGCAACGGACATC-3′; *Rpn3*-Rev, 5′-TTAGAAACC-ATCCTCATCATCCTC-3′; *Rpt1*-For, 5′-CACCATGCCGGACTACCTGGGCGAC-3′, *Rpt1*-Rev, 5′-TTAGTTGTAGGTCATGTAGCGTG-3′. The PCR products were cloned into pENTR (Life Technologies) and swapped into pAFW (*Drosophila* Gateway Vector Collection) using an LR reaction.

To generate the inducible HA-Ipo9^{FL} and HA-Ipo9$^{\Delta N(36\text{-}144aa)}$, the open reading frames were amplified using primers (forward, 5′-tccagtgtggtggaattctgcagatAGCCACCATGGATCTCCACCGCGGTGGA-3′ and reverse, 5′-acagtcgaggctgatcagcgggtttCTACTTCTGCTGGACCTTGCTG-3′) off of a ppHW template containing the *Ipo9^{FL}* or *Ipo9$^{\Delta N}$* sequence. The PCR products were cloned into the pMT vector using a NEBuilder HiFi DNA Assembly kit to generate N-terminal 3×HA tagged proteins under control of the metallothionein promoter.

Transient transfections of S2 cells were performed using Effectene Transfection Reagent (Qiagen) following the manufacturer's instructions. After 16 h of induction with CuSO4 (0.7 mM), S2 cells were lysed on ice in lysis buffer. Rat anti-HA Affinity Matrix (Roche) was incubated with lysates for 3 h at 4°C. The beads were then quickly washed six times with lysis buffer and boiled in Laemmli sample buffer with 10% BME.

Expression and purification of recombinant Ipo9 and proteasome proteins

To generate the inducible FLAG-tagged proteins, we amplified fragments from previously cloned cDNA constructs using the following set of primers: Common Forward, 5′-GAAGGAGATATACCATGGGCAGCAGCAGCCAAGACTACAAAGACCATGACGGT-3′ and either *Prosα6T*-REV, 5′-CTTTCTGTTCGACTTAAGCATTATGCTCAATGTGCGTCACTGCCGC-3′; *Prosα2*-REV, 5′-CTTTCTGTTCGACTTAAGCATTATGCTTAGGGGATGCTGGCCAAGT-3′; *Rpn1*-REV, 5′-CTTTCTGTTCGACTTAAGCATTATGCCTATTTCACAAAATTTGGGTTCTT; *Rpn*- REV, 5′-CTTTCTGTTCGACTTAAGCATTATGCTTAGAAACCATCCTCATCATCCTC-3′; and *Rpt1*-REV 5′ CTTTCTGTTCGACTTAAGCATTATGCTTAGTTGTAGGTCATGTAGCGT. The PCR products were then recombined into the VC024 vector using a NEBuilder HiFi DNA Assembly kit to generate N-terminal 3×Flag tag proteins under lac operator. The VC024 vector was a gift from Victor Cruz (Erzberger Lab, University of Texas Southwestern, TX, USA).

To generate the inducible N-terminal 6XHis Ipo9, PCR was carried out using primers 5′-GAGGTCTTATTTCAAGGCCCGGGAGGTAGTGGAAGCTCGCTGCAATTCCAAAACGAC-3′ (forward) and 5′ GGCCCCAAGGGGTTATGCTAGTTATTGCCTACTTCTGCTGGACCTTGCTG-3′ (reverse) using *Ipo9* cDNA. The PCR product was then cloned into the VC024 vector using a NEBuilder HiFi DNA Assembly kit to generate N-terminal 6XHis Ipo9 under lac operator and sequence verified.

BL21(DE3) *Escherichia coli* cells were transformed with VC024- Flag-Prosα6T, VC024-Flag-Prosα2, VC024-Flag-Rpn1, VC024-Flag-Rpn3, VC024-Flag-Rpt1 or VC024-His-Ipo9 plasmids and grown at 37°C in LB media under ampicillin selection until the OD_{600} reached ∼0.6-0.7 absorbance units. Cultures were induced with final concentrations of 5 mM isopropyl β-D-1-thiogalactopyranoside (IPTG) and incubated with shaking overnight at room temperature (20-22°C).

The following buffers were used for Ni-NTA purification of Ipo9: resuspension buffer, 50 mM Tris (pH 7.5), 200 mM NaCl, 10% glycerol, 1 mM DTT, 1 mM EDTA, 5 mM imidazole and protease inhibitors; wash buffer, 50 mM Tris (pH 7.5), 200 mM NaCl, 10% glycerol, 1 mM DTT, 1 mM EDTA and 30 mM imidazole; and elution buffer, 50 mM Tris (pH 7.5), 200 mM NaCl, 10% glycerol, 1 mM DTT, 1 mM EDTA and 250 mM imidazole.

Overnight cultures were pelleted by centrifugation at 3000 ***g*** for 25 min at 4°C. Cells were resuspended in 1 ml of the appropriate resuspension buffer. The samples were sonicated using 30 s pulses with 59 s rest times for a total 'on' process time of 1 min and 30 s. The resulting lysate was spun at 20,000 ***g*** for 30 min at 4°C. The supernatants were collected, mixed and incubated with 0.25 ml of Ni-NTA resin (previously washed with resuspension buffer) at 4°C with nutating for 30 min to 1 h. The beads were then washed with 15 ml of the appropriate wash buffer. Finally, proteins were eluted using 0.25 ml of elution buffer.

Statistics

No statistical methods were used to predetermine sample size. The experiments were not randomized. The investigators were not blinded to allocation during experiments and outcome assessment. The experiments were performed in biological triplicates except for those featured in Fig. S3L. Statistical analysis and graphing were performed using Microsoft Excel 2010 and GraphPad Prism 9 software. Data are mean±s.d. The *P*-value (two-tailed Student's *t*-test) is provided for comparison with the control shown as $*P \leq 0.05$, $**P \leq 0.01$, $***P \leq 0.001$, and n.s., not significant ($P > 0.05$).

Oligos and key resources

Oligos used in the study are listed in Table S1. Detailed information about key resources is provided in Table S2.

Acknowledgements

We thank K. McKim, A. Ephrussi, Y. Yamashita, M. Lilly, J. Belote, R. Glaser, the Bloomington *Drosophila* Stock Center and the Developmental Studies Hybridoma Bank for reagents. We thank previous and current members of the Buszczak laboratory for comments and advice.

Competing interests

The authors declare no competing or financial interests.

Author contributions

Conceptualization: V.P., M.B.; Methodology: V.P., T.L.T., M.B.; Validation: V.P., M.B.; Formal analysis: V.P., T.L.T.; Investigation: V.P., G.C.K., M.B.; Resources: M.B.; Writing - original draft: V.P., M.B.; Writing - review & editing: V.P., T.L.T., M.B.; Visualization: M.B.; Supervision: T.L.T., M.B.; Project administration: M.B.; Funding acquisition: T.L.T., M.B.

Funding

This work was funded by the National Institutes of Health (R01GM116885 to T.L.T. and R01GM125812 and R01AG047318 to M.B.). Deposited in PMC for release after 12 months.

Supplementary information

Supplementary information available online at
https://jcs.biologists.org/lookup/doi/10.1242/jcs.258391.supplemental

References

Arama, E., Bader, M., Rieckhof, G. E. and Steller, H. (2007). A ubiquitin ligase complex regulates caspase activation during sperm differentiation in Drosophila. *PLoS Biol.* **5**, e251. doi:10.1371/journal.pbio.0050251

Awe, S. and Renkawitz-Pohl, R. (2010). Histone H4 acetylation is essential to proceed from a histone- to a protamine-based chromatin structure in spermatid nuclei of Drosophila melanogaster. *Syst. Biol. Reprod Med.* **56**, 44-61. doi:10.3109/19396360903490790

Baker, S. E., Lorenzen, J. A., Miller, S. W., Bunch, T. A., Jannuzi, A. L., Ginsberg, M. H., Perkins, L. A. and Brower, D. L. (2002). Genetic interaction between integrins and moleskin, a gene encoding a Drosophila homolog of importin-7. *Genetics* **162**, 285-296.

Bange, G., Murat, G., Sinning, I., Hurt, E. and Kressler, D. (2013). New twist to nuclear import: when two travel together. *Commun. Integr. Biol.* **6**, e24792. doi:10.4161/cib.24792

Belin, B. J., Lee, T. and Mullins, R. D. (2015). DNA damage induces nuclear actin filament assembly by Formin −2 and Spire-(1/2) that promotes efficient DNA repair. [corrected]. *Elife* **4**, e07735. doi:10.7554/eLife.07735

Beliveau, B. J., Apostolopoulos, N. and Wu, C. T. (2014). Visualizing genomes with Oligopaint FISH probes. *Curr. Protoc. Mol. Biol.* **105**, Unit 14 23. doi:10.1002/0471142727.mb1423s105

Beliveau, B. J., Boettiger, A. N., Avendano, M. S., Jungmann, R., McCole, R. B., Joyce, E. F., Kim-Kiselak, C., Bantignies, F., Fonseka, C. Y., Erceg, J. et al. (2015). Single-molecule super-resolution imaging of chromosomes and in situ haplotype visualization using Oligopaint FISH probes. *Nat. Commun.* **6**, 7147. doi:10.1038/ncomms8147

Beliveau, B. J., Joyce, E. F., Apostolopoulos, N., Yilmaz, F., Fonseka, C. Y., McCole, R. B., Chang, Y., Li, J. B., Senaratne, T. N., Williams, B. R. et al. (2012). Versatile design and synthesis platform for visualizing genomes with Oligopaint FISH probes. *Proc. Natl. Acad. Sci. USA* **109**, 21301-21306. doi:10.1073/pnas.1213818110

Cagan, R. L. (2003). Spermatogenesis: borrowing the apoptotic machinery. *Curr. Biol.* **13**, R600-R602. doi:10.1016/s0960-9822(03)00525-6

Çağatay, T. and Chook, Y. M. (2018). Karyopherins in cancer. *Curr. Opin. Cell Biol.* **52**, 30-42. doi:10.1016/j.ceb.2018.01.006

Cautain, B., Hill, R., de Pedro, N. and Link, W. (2015). Components and regulation of nuclear transport processes. *FEBS J.* **282**, 445-462. doi:10.1111/febs.13163

Chi, N. C. and Adam, S. A. (1997). Functional domains in nuclear import factor p97 for binding the nuclear localization sequence receptor and the nuclear pore. *Mol. Biol. Cell* **8**, 945-956. doi:10.1091/mbc.8.6.945

Chook, Y. M. and Blobel, G. (2001). Karyopherins and nuclear import. *Curr. Opin. Struct. Biol.* **11**, 703-715. doi:10.1016/S0959-440X(01)00264-0

Collier, S., Chan, H. Y., Toda, T., McKimmie, C., Johnson, G., Adler, P. N., O'Kane, C. and Ashburner, M. (2000). The Drosophila embargoed gene is required for larval progression and encodes the functional homolog of schizosaccharomyces Crm1. *Genetics* **155**, 1799-1807.

Dopie, J., Skarp, K.-P., Rajakyla, E. K., Tanhuanpaa, K. and Vartiainen, M. K. (2012). Active maintenance of nuclear actin by importin 9 supports transcription. *Proc. Natl. Acad. Sci. USA* **109**, E544-E552. doi:10.1073/pnas.1118880109

Fabian, L. and Brill, J. A. (2012). Drosophila spermiogenesis: Big things come from little packages. *Spermatogenesis* **2**, 197-212. doi:10.4161/spmg.21798

Fried, H. and Kutay, U. (2003). Nucleocytoplasmic transport: taking an inventory. *Cell. Mol. Life Sci.* **60**, 1659-1688. doi:10.1007/s00018-003-3070-3

Fujii, K., Miyata, Y., Takahashi, I., Koizumi, H., Saji, H., Hoshikawa, M., Takagi, M., Nishimura, T. and Nakamura, H. (2018). Differential proteomic analysis between small cell lung carcinoma (SCLC) and pulmonary carcinoid tumors reveals molecular signatures for malignancy in lung cancer. *Proteomics Clin. Appl.* **12**, e1800015. doi:10.1002/prca.201800015

Giagtzoglou, N., Lin, Y. Q., Haueter, C. and Bellen, H. J. (2009). Importin 13 regulates neurotransmitter release at the Drosophila neuromuscular junction. *J. Neurosci.* **29**, 5628-5639. doi:10.1523/JNEUROSCI.0794-09.2009

Giarrè, M., Török, I., Schmitt, R., Gorjánácz, M., Kiss, I. and Mechler, B. M. (2002). Patterns of importin-alpha expression during Drosophila spermatogenesis. *J. Struct. Biol.* **140**, 279-290. doi:10.1016/S1047-8477(02)00543-9

Gontan, C., Güttler, T., Engelen, E., Demmers, J., Fornerod, M., Grosveld, F. G., Tibboel, D., Gorlich, D., Poot, R. A. and Rottier, R. J. (2009). Exportin 4 mediates a novel nuclear import pathway for Sox family transcription factors. *J. Cell Biol.* **185**, 27-34. doi:10.1083/jcb.200810106

Gratz, S. J., Cummings, A. M., Nguyen, J. N., Hamm, D. C., Donohue, L. K., Harrison, M. M., Wildonger, J. and O'Connor-Giles, K. M. (2013). Genome engineering of Drosophila with the CRISPR RNA-guided Cas9 nuclease. *Genetics* **194**, 1029-1035. doi:10.1534/genetics.113.152710

Gratz, S. J., Ukken, F. P., Rubinstein, C. D., Thiede, G., Donohue, L. K., Cummings, A. M. and O'Connor-Giles, K. M. (2014). Highly specific and efficient CRISPR/Cas9-catalyzed homology-directed repair in Drosophila. *Genetics* **196**, 961-971. doi:10.1534/genetics.113.160713

Guruharsha, K. G., Rual, J.-F., Zhai, B., Mintseris, J., Vaidya, P., Vaidya, N., Beekman, C., Wong, C., Rhee, D. Y., Cenaj, O. et al. (2011). A protein complex network of Drosophila melanogaster. *Cell* **147**, 690-703. doi:10.1016/j.cell.2011.08.047

Higashi-Kovtun, M. E., Mosca, T. J., Dickman, D. K., Meinertzhagen, I. A. and Schwarz, T. L. (2010). Importin-beta11 regulates synaptic phosphorylated mothers against decapentaplegic, and thereby influences synaptic development and function at the Drosophila neuromuscular junction. *J. Neurosci.* **30**, 5253-5268. doi:10.1523/JNEUROSCI.3739-09.2010

Hong, A., Lee-Kong, S., Iida, T., Sugimura, I. and Lilly, M. A. (2003). The p27cip/kip ortholog dacapo maintains the Drosophila oocyte in prophase of meiosis I. *Development* **130**, 1235-1242. doi:10.1242/dev.00352

Hughes, S. E., Miller, D. E., Miller, A. L. and Hawley, R. S. (2018). Female meiosis: synapsis, recombination, and segregation in Drosophila melanogaster. *Genetics* **208**, 875-908. doi:10.1534/genetics.117.300081

Ilius, M., Wolf, R. and Heisenberg, M. (2007). The central complex of Drosophila melanogaster is involved in flight control: studies on mutants and mosaics of the gene ellipsoid body open. *J. Neurogenet.* **21**, 321-338. doi:10.1080/01677060701693503

Jäckel, S., Summerer, A. K., Thömmes, C. M., Pan, X., Voigt, A., Schulz, J. B., Rasse, T. M., Dormann, D., Haass, C. and Kahle, P. J. (2015). Nuclear import factor transportin and arginine methyltransferase 1 modify FUS neurotoxicity in Drosophila. *Neurobiol. Dis.* **74**, 76-88. doi:10.1016/j.nbd.2014.11.003

Jakel, S. and Gorlich, D. (1998). Importin beta, transportin, RanBP5 and RanBP7 mediate nuclear import of ribosomal proteins in mammalian cells. *EMBO J.* **17**, 4491-4502. doi:10.1093/emboj/17.15.4491

Kahsai, L., Millburn, G. H. and Cook, K. R. (2016). Phenotypes associated with second chromosome P element insertions in Drosophila melanogaster. *G3 (Bethesda)* **6**, 2665-2670. doi:10.1534/g3.116.030940

Kaplan, Y., Gibbs-Bar, L., Kalifa, Y., Feinstein-Rotkopf, Y. and Arama, E. (2010). Gradients of a ubiquitin E3 ligase inhibitor and a caspase inhibitor determine differentiation or death in spermatids. *Dev. Cell* **19**, 160-173. doi:10.1016/j.devcel.2010.06.009

Kelpsch, D. J., Groen, C. M., Fagan, T. N., Sudhir, S. and Tootle, T. L. (2016). Fascin regulates nuclear actin during Drosophila oogenesis. *Mol. Biol. Cell* **27**, 2965-2979. doi:10.1091/mbc.E15-09-0634

Kimura, M. and Imamoto, N. (2014). Biological significance of the importin-β family-dependent nucleocytoplasmic transport pathways. *Traffic* **15**, 727-748. doi:10.1111/tra.12174

Kimura, M., Morinaka, Y., Imai, K., Kose, S., Horton, P. and Imamoto, N. (2017). Extensive cargo identification reveals distinct biological roles of the 12 importin pathways. *Elife* **6**, e21184. doi:10.7554/eLife.21184.035

Kortvely, E., Burkovics, P., Varszegi, S. and Gulya, K. (2005). Cloning and characterization of rat importin 9: implication for its neuronal function. *Brain Res. Mol. Brain Res.* **139**, 103-114. doi:10.1016/j.molbrainres.2005.05.021

Kutay, U., Izaurralde, E., Bischoff, F. R., Mattaj, I. W. and Gorlich, D. (1997). Dominant-negative mutants of importin-beta block multiple pathways of import and export through the nuclear pore complex. *EMBO J.* **16**, 1153-1163. doi:10.1093/emboj/16.6.1153

Lippai, M., Tirian, L., Boros, I., Mihaly, J., Erdelyi, M., Belecz, I., Máthé, E., Posfai, J., Nagy, A., Udvardy, A. et al. (2000). The Ketel gene encodes a Drosophila homologue of importin-beta. *Genetics* **156**, 1889-1900.

Mahipal, A. and Malafa, M. (2016). Importins and exportins as therapeutic targets in cancer. *Pharmacol. Ther.* **164**, 135-143. doi:10.1016/j.pharmthera.2016.03.020

Major, A. T., Whiley, P. A. and Loveland, K. L. (2011). Expression of nucleocytoplasmic transport machinery: clues to regulation of spermatogenic development. *Biochim. Biophys. Acta* **1813**, 1668-1688. doi:10.1016/j.bbamcr.2011.03.008

Mani, S. R., Megosh, H., and Lin, H. (2014). Piwi proteins are essential for early Drosophila embryogenesis. *Dev. Biol.* **385**, 340-349. doi:10.1016/j.ydbio.2013.10.017

Mansfield, E., Hersperger, E., Biggs, J. and Shearn, A. (1994). Genetic and molecular analysis of hyperplastic discs, a gene whose product is required for regulation of cell proliferation in Drosophila melanogaster imaginal discs and germ cells. *Dev. Biol.* **165**, 507-526. doi:10.1006/dbio.1994.1271

Mason, D. A., Fleming, R. J. and Goldfarb, D. S. (2002). Drosophila melanogaster importin alpha1 and alpha3 can replace importin alpha2 during spermatogenesis but not oogenesis. *Genetics* **161**, 157-170.

Máthé, E., Bates, H., Huikeshoven, H., Deák, P., Glover, D. M. and Cotterill, S. (2000). Importin-α3 is required at multiple stages of Drosophila development and has a role in the completion of oogenesis. *Dev. Biol.* **223**, 307-322. doi:10.1006/dbio.2000.9743

Matsumiya, T., Xing, F., Ebina, M., Hayakari, R., Imaizumi, T., Yoshida, H., Kikuchi, H., Topham, M. K., Satoh, K. and Stafforini, D. M. (2013). Novel role for molecular transporter importin 9 in posttranscriptional regulation of IFN-ε expression. *J. Immunol.* **191**, 1907-1915. doi:10.4049/jimmunol.1201925

Natalizio, A. H. and Matera, A. G. (2013). Identification and characterization of Drosophila Snurportin reveals a role for the import receptor Moleskin/importin-7 in snRNP biogenesis. *Mol. Biol. Cell* **24**, 2932-2942. doi:10.1091/mbc.e13-03-0118

Padavannil, A., Sarkar, P., Kim, S. J., Cagatay, T., Jiou, J., Brautigam, C. A., Tomchick, D. R., Sali, A., D'Arcy, S. and Chook, Y. M. (2019). Importin-9 wraps around the H2A-H2B core to act as nuclear importer and histone chaperone. *Elife* **8**, e43630. doi:10.7554/eLife.43630.030

Plafker, S. M. and Macara, I. G. (2002). Ribosomal protein L12 uses a distinct nuclear import pathway mediated by importin 11. *Mol. Cell. Biol.* **22**, 1266-1275. doi:10.1128/MCB.22.4.1266-1275.2002

Quan, Y., Ji, Z. L., Wang, X., Tartakoff, A. M. and Tao, T. (2008). Evolutionary and transcriptional analysis of karyopherin beta superfamily proteins. *Mol. Cell. Proteomics* **7**, 1254-1269. doi:10.1074/mcp.M700511-MCP200

Radford, S. J. and McKim, K. S. (2016). Techniques for imaging prometaphase and metaphase of meiosis I in fixed Drosophila oocytes. *J Vis Exp.* **116**, 54666. doi:10.3791/54666

Rathke, C., Baarends, W. M., Jayaramaiah-Raja, S., Bartkuhn, M., Renkawitz, R. and Renkawitz-Pohl, R. (2007). Transition from a nucleosome-based to a protamine-based chromatin configuration during spermiogenesis in Drosophila. *J. Cell Sci.* **120**, 1689-1700. doi:10.1242/jcs.004663

Rathke, C., Barckmann, B., Burkhard, S., Jayaramaiah-Raja, S., Roote, J. and Renkawitz-Pohl, R. (2010). Distinct functions of Mst77F and protamines in nuclear shaping and chromatin condensation during Drosophila spermiogenesis. *Eur. J. Cell Biol.* **89**, 326-338. doi:10.1016/j.ejcb.2009.09.001

Rathke, C., Baarends, W. M., Awe, S. and Renkawitz-Pohl, R. (2014). Chromatin dynamics during spermiogenesis. *Biochim. Biophys. Acta* **1839**, 155-168. doi:10.1016/j.bbagrm.2013.08.004

Schupbach, T. and Wieschaus, E. (1991). Female sterile mutations on the second chromosome of Drosophila melanogaster. II. Mutations blocking oogenesis or altering egg morphology. *Genetics* **129**, 1119-1136. doi:10.1093/genetics/129.4.1119

Sokolova, M., Moore, H. M., Prajapati, B., Dopie, J., Merilainen, L., Honkanen, M., Matos, R. C., Poukkula, M., Hietakangas, V. and Vartiainen, M. K. (2018). Nuclear actin is required for transcription during drosophila oogenesis. *iScience* **9**, 63-70. doi:10.1016/j.isci.2018.10.010

Soniat, M., Cagatay, T. and Chook, Y. M. (2016). Recognition elements in the histone H3 and H4 tails for seven different importins. *J. Biol. Chem.* **291**, 21171-21183. doi:10.1074/jbc.M116.730218

Ström, A.-C. and Weis, K. (2001). Importin-beta-like nuclear transport receptors. *Genome Biol.* **2**, Reviews3008. doi:10.1186/gb-2001-2-6-reviews3008

Tekotte, H., Berdnik, D., Török, T., Buszczak, M., Jones, L. M., Cooley, L., Knoblich, J. A. and Davis, I. (2002). Dcas is required for importin-alpha3 nuclear export and mechano-sensory organ cell fate specification in Drosophila. *Dev. Biol.* **244**, 396-406. doi:10.1006/dbio.2002.0612

Timinszky, G., Tirian, L., Nagy, F. T., Toth, G., Perczel, A., Kiss-Laszlo, Z., Boros, I., Clarke, P. R. and Szabad, J. (2002). The importin-beta P446L dominant-negative mutant protein loses RanGTP binding ability and blocks the formation of intact nuclear envelope. *J. Cell Sci.* **115**, 1675-1687.

Tirian, L., Puro, J., Erdelyi, M., Boros, I., Papp, B., Lippai, M. and Szabad, J. (2000). The Ketel(D) dominant-negative mutations identify maternal function of the Drosophila importin-beta gene required for cleavage nuclei formation. *Genetics* **156**, 1901-1912.

Turner, J. G., Dawson, J. and Sullivan, D. M. (2012). Nuclear export of proteins and drug resistance in cancer. *Biochem. Pharmacol.* **83**, 1021-1032. doi:10.1016/j.bcp.2011.12.016

Turner, J. G., Dawson, J., Cubitt, C. L., Baz, R. and Sullivan, D. M. (2014). Inhibition of CRM1-dependent nuclear export sensitizes malignant cells to cytotoxic and targeted agents. *Semin. Cancer Biol.* **27**, 62-73. doi:10.1016/j.semcancer.2014.03.001

VanKuren, N. W. and Long, M. (2018). Gene duplicates resolving sexual conflict rapidly evolved essential gametogenesis functions. *Nat Ecol Evol* **2**, 705-712. doi:10.1038/s41559-018-0471-0

White-Cooper, H. (2004). Spermatogenesis: analysis of meiosis and morphogenesis. *Methods Mol. Biol.* **247**, 45-75. doi:10.1385/1-59259-665-7:45

White-Cooper, H. (2010). Molecular mechanisms of gene regulation during Drosophila spermatogenesis. *Reproduction* **139**, 11-21. doi:10.1530/REP-09-0083

Wineland, D. M., Kelpsch, D. J. and Tootle, T. L. (2018). Multiple pools of nuclear actin. *Anat. Rec. (Hoboken)* **301**, 2014-2036. doi:10.1002/ar.23964

Zhong, L. and Belote, J. M. (2007). The testis-specific proteasome subunit Prosalpha6T of D. melanogaster is required for individualization and nuclear maturation during spermatogenesis. *Development* **134**, 3517-3525. (doi:10.1242/dev.004770)

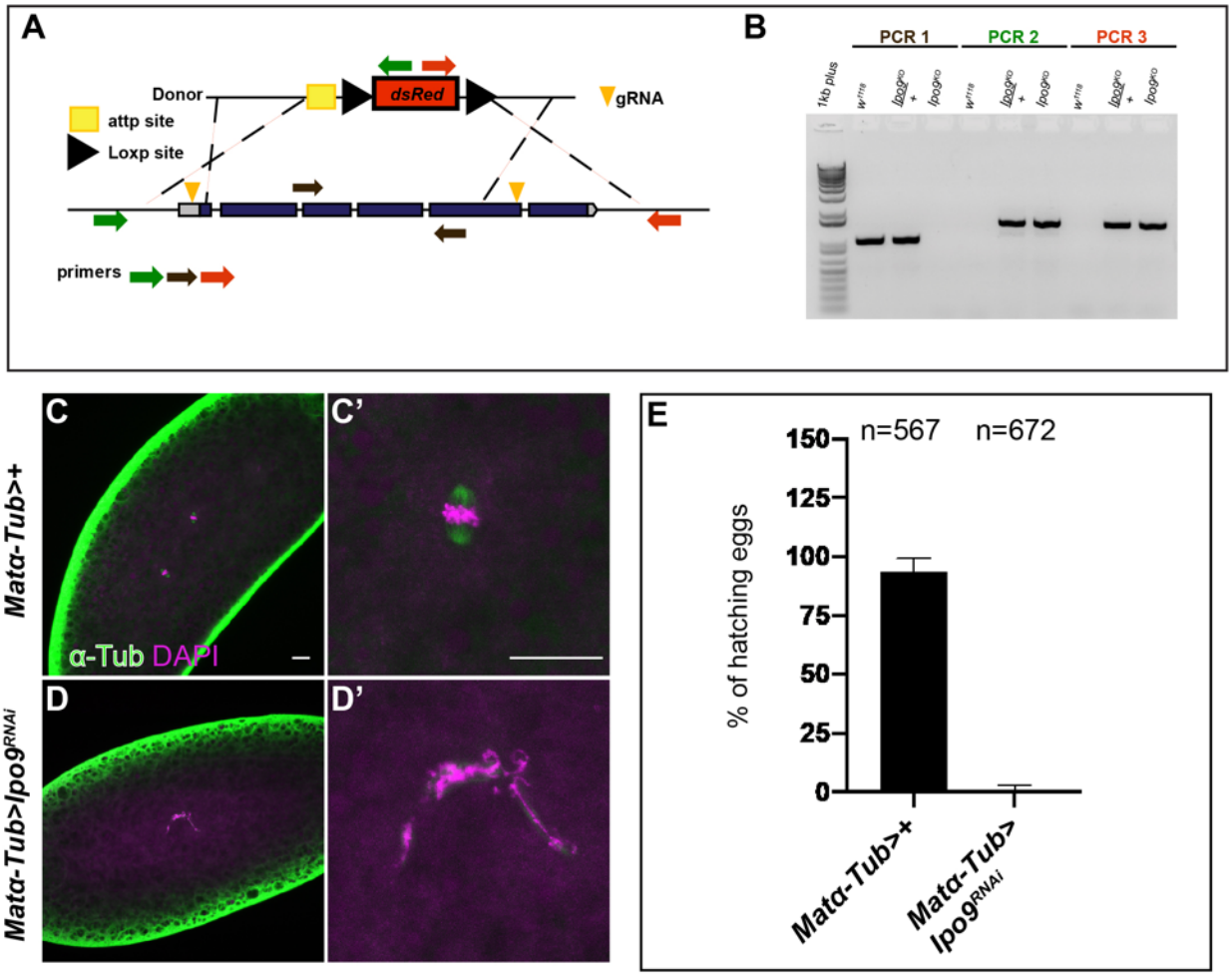

Figure S1. Loss of *Ipo9* in germ cells results in fertility defects (A) Schematic of strategy used to knock-in 3xP3-dsRed cassette to replace the majority of *Ipo9* sequence. (B) PCR verification (color coded according to primers marked by the arrows in panel A) of knock-in of *3xP3-dsRed* cassette into the *Ipo9* locus in the $Ipo9^{KO}$ allele. (C-C') Embryos from *Mat-α-Tub-gal4* (control) and (D-D') *Mat-α-Tub-gal4>*$Ipo9^{RNAi}$ mothers stained for α-Tub (green) and DAPI (magenta). (E) Percentage of eggs that hatch after 5 days of being laid by *Mat-α-Tub-gal4* (control) and *Mat-α-Tub-gal4 >*$Ipo9^{RNAi}$ females crossed to w^{1118} males. Scale bars 20µm.

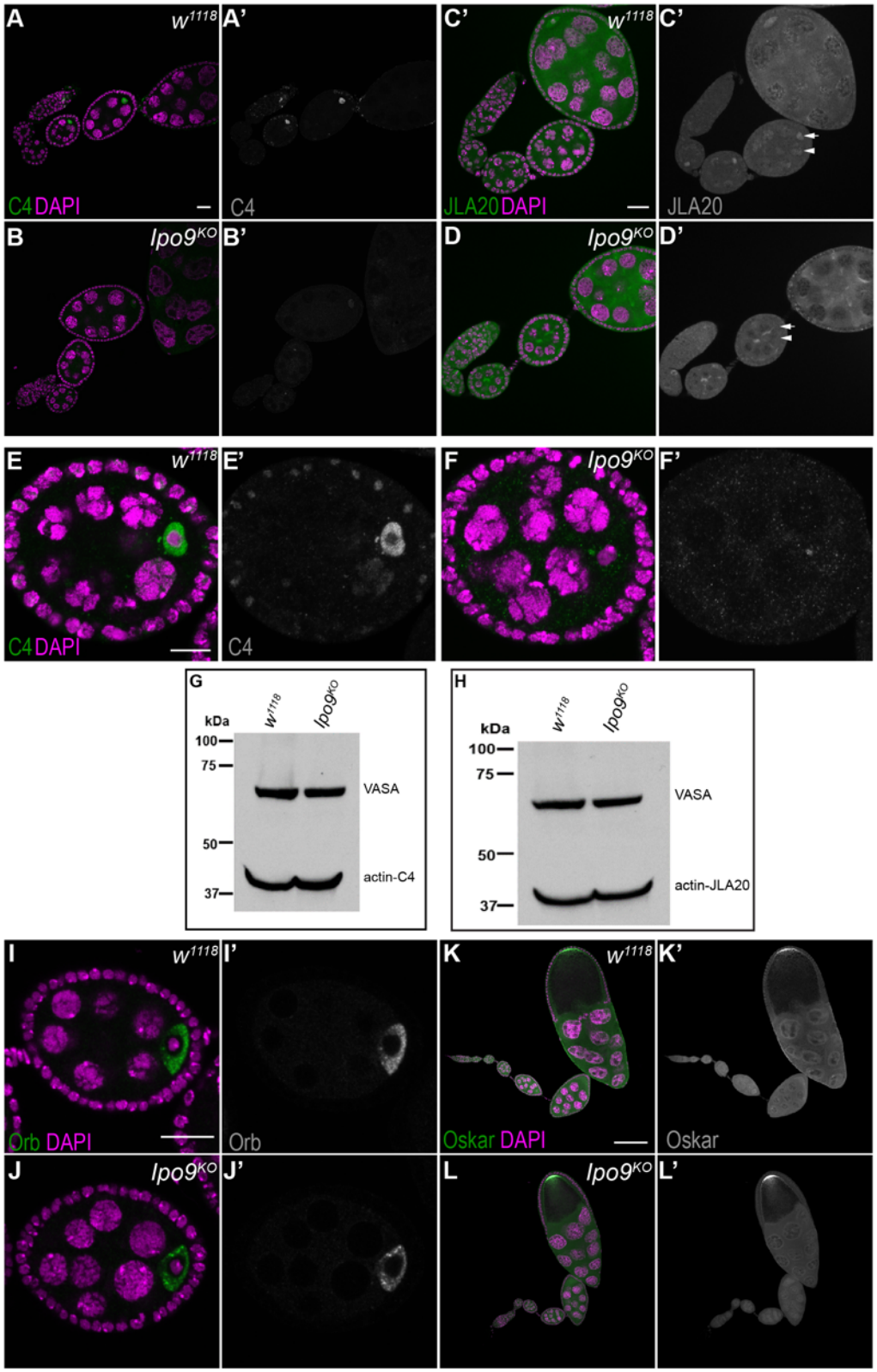

Figure S2. *lpo9*^{KO} germ cells show a reduction of nuclear actin. (A-B) Ovarioles stained using anti-Actin-C4 antibodies (green) and DAPI (magenta). (A-A') *w*^{1118} (control) and (B-B') *lpo9*^{KO}. (C-D) Ovarioles stained using anti-Actin-JLA20 antibodies (green) and DAPI (magenta). (C-C') *w*^{1118}

(control) and (D-D') *Ipo9*^{KO} ovariole. Scale bars 20 μm. (E-F) Stage 4 egg chambers stained using anti-Actin-C4 antibodies (green) and DAPI (magenta). (E-E') *w*^{1118} (control) and (F-F') *Ipo9*^{KO}. Scale bars 10μm. (G) Western blot showing Actin (C4) and Vasa abundance from *w*^{1118} (control) and *Ipo9*^{KO} ovaries. (H) Western blot from showing Actin (ActinJLA20) and Vasa abundance from *w*^{1118} (control) and *Ipo9*^{KO} ovaries. (I, I') *w*^{1118} control and (J,J') *Ipo9*^{KO} egg chambers stained for Orb (green) and DNA (magenta). (K, K') *w*^{1118} control and (L,L') *Ipo9*^{KO} egg chambers stained for Oskar (green) and DNA (magenta). Both Orb and Oskar localize to the oocyte in Ipo9 mutant egg chambers, indicating that general transport to the oocyte is not disrupted. Scale bar in I-J' represents 20 μm and in K-L' 100 μm.

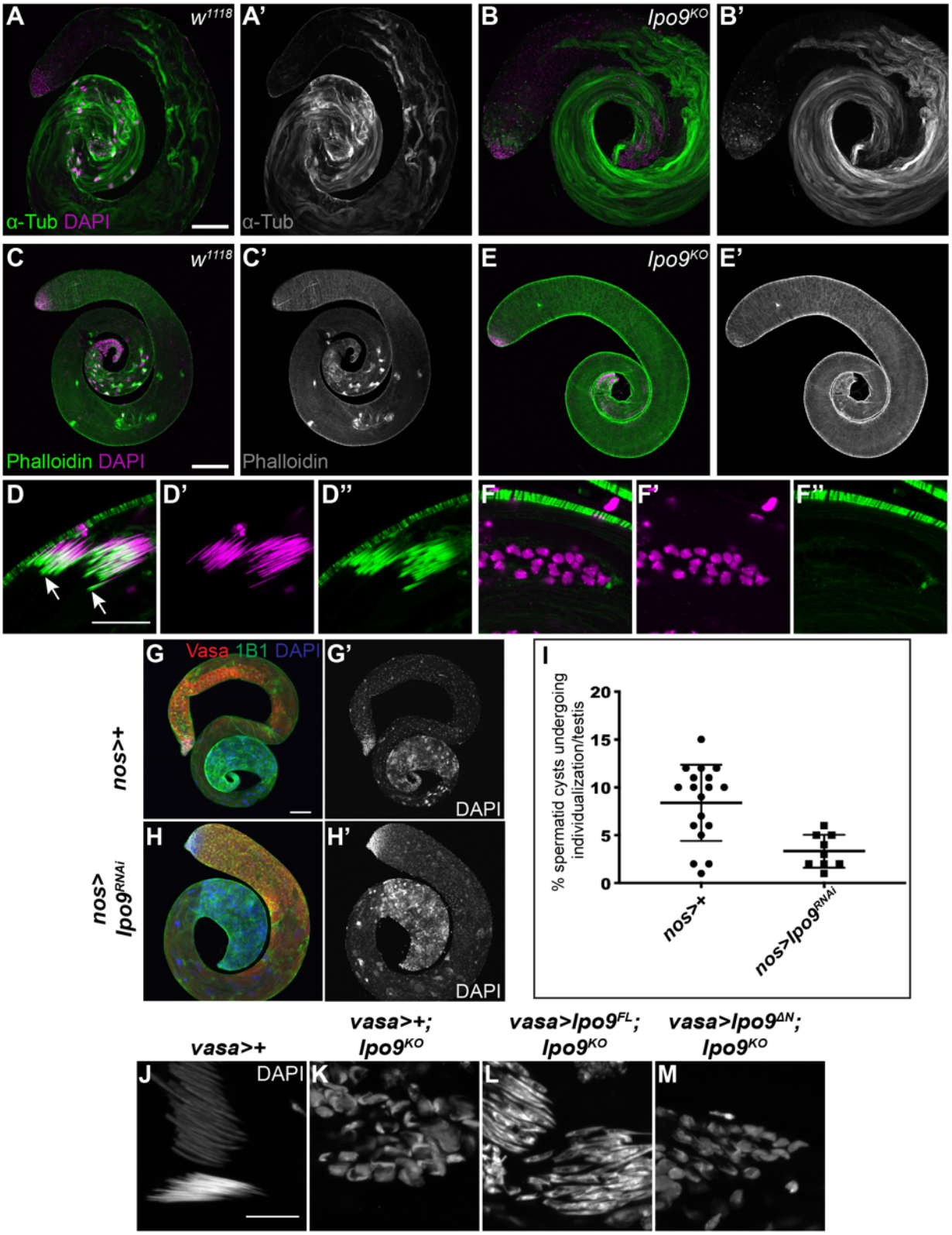

Figure S3. *lpo9*^{KO} nuclei are unable to individualize.
(A-B') Testes stained for α-Tub (green) and DAPI (magenta). (A-A') *w*^{1118} testis and (B-B') *lpo9*^{KO} testis. (C-F") Testes stained for phalloidin (green) and DAPI (magenta). (C-D) *w*^{1118} testis and nuclei

(arrows pointing actin cones) and (E-F') *Ipo9*^{KO} testis and nuclei. Scale bars 20μm. (G-G') A *Maternal Triple Driver* (*MTD)-gal4* (control) and (H-H') *MTD-gal4>Ipo9*^{RNAi} *Drosophila* testes stained for VASA (red), 1B1 (green) and DAPI (blue). Scale bars 20μm. (I) Percentage of spermatid cysts undergoing individualization from *MTD-gal4* (control) and *MTD-gal4>Ipo9*^{RNAi} males. Bars represent the mean and standard deviation. (J-M) Elongating sperm stained with DAPI (gray) for these genotypes (J) *vasa-gal4>;+*, (K) *vasa-gal4>;Ipo9*^{KO}, (L) *vasa-gal4>Ipo9*^{FL}*;Ipo9*^{KO} and (M) *vasa-gal4>Ipo9*$^{\Delta N}$*;Ipo9*^{KO}. Scale bars represent 10μm.

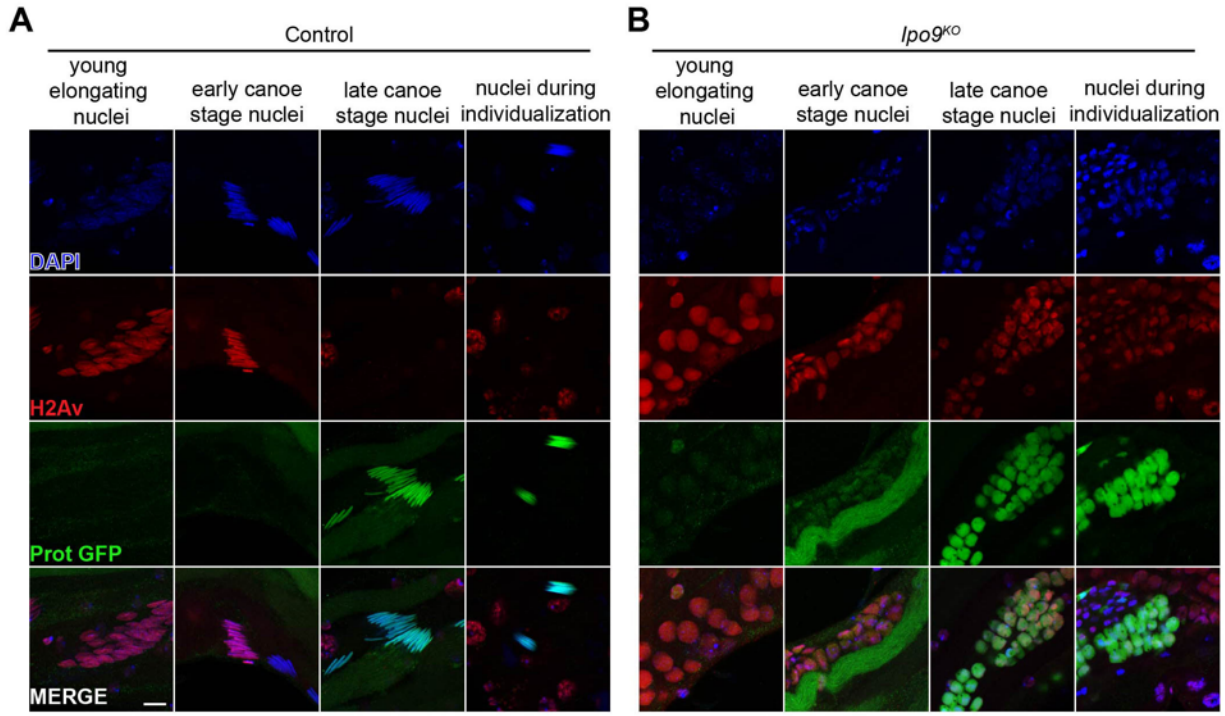

Figure S4. *Ipo9*^{KO} spermatids show defect in H2Av removal.
(A-B) Elongating nuclei stained for H2Av-RFP (red), ProtB-GFP (green) and DAPI (blue). (A) *w*^{1118} nuclei are able to elongate and replace histone with protamineB. (B) *Ipo9*^{KO} nuclei are unable to elongate and properly remove histones. Scale bars 10μm.

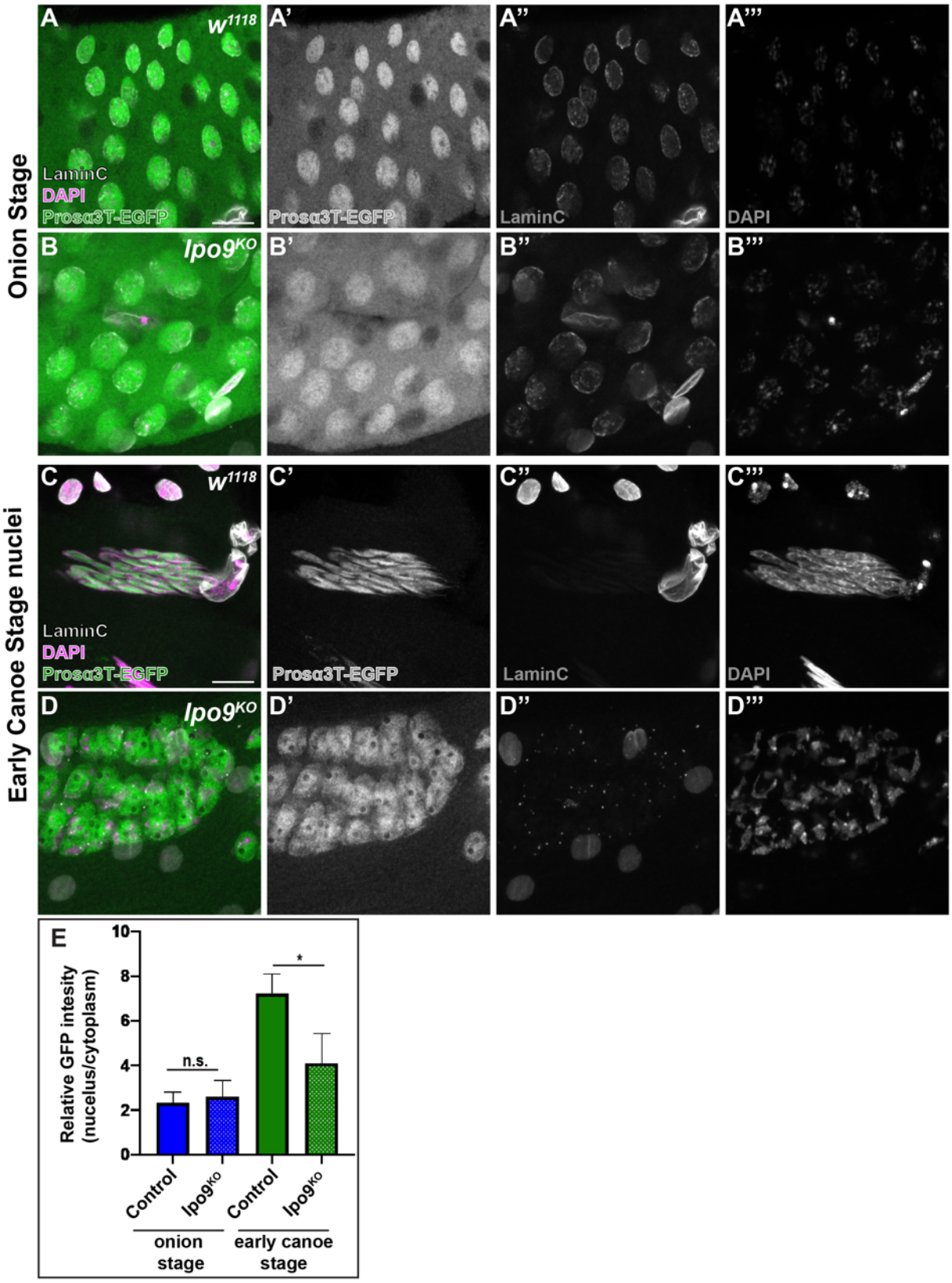

Figure S5. *Ipo9*^{KO} spermatids show reduction of Prosα3T in the nucleus. (A-D) Spermatids at the onion stage and early canoe stage, stained for Prosα3T-EGFP (green), LaminC (red) and DNA

(blue). (A & C) w^{1118} spermatids and (B & D) $Ipo9^{KO}$ spermatids. (E) Quantification of relative fluorescent intensity of Prosa3T-EGFP in the nuclei and cytoplasm of control and $Ipo9^{KO}$ samples. n=40 for each genotype at the onion stage and n=45 for each genotype at early canoe stage. Average values and standard deviations are shown on the graph. *P*-values from t-tests are provided as *P ≤0.05, **P≤0.01, ***P≤0.00; NS, non-significant (P>0.05).Scale bars 10μm.

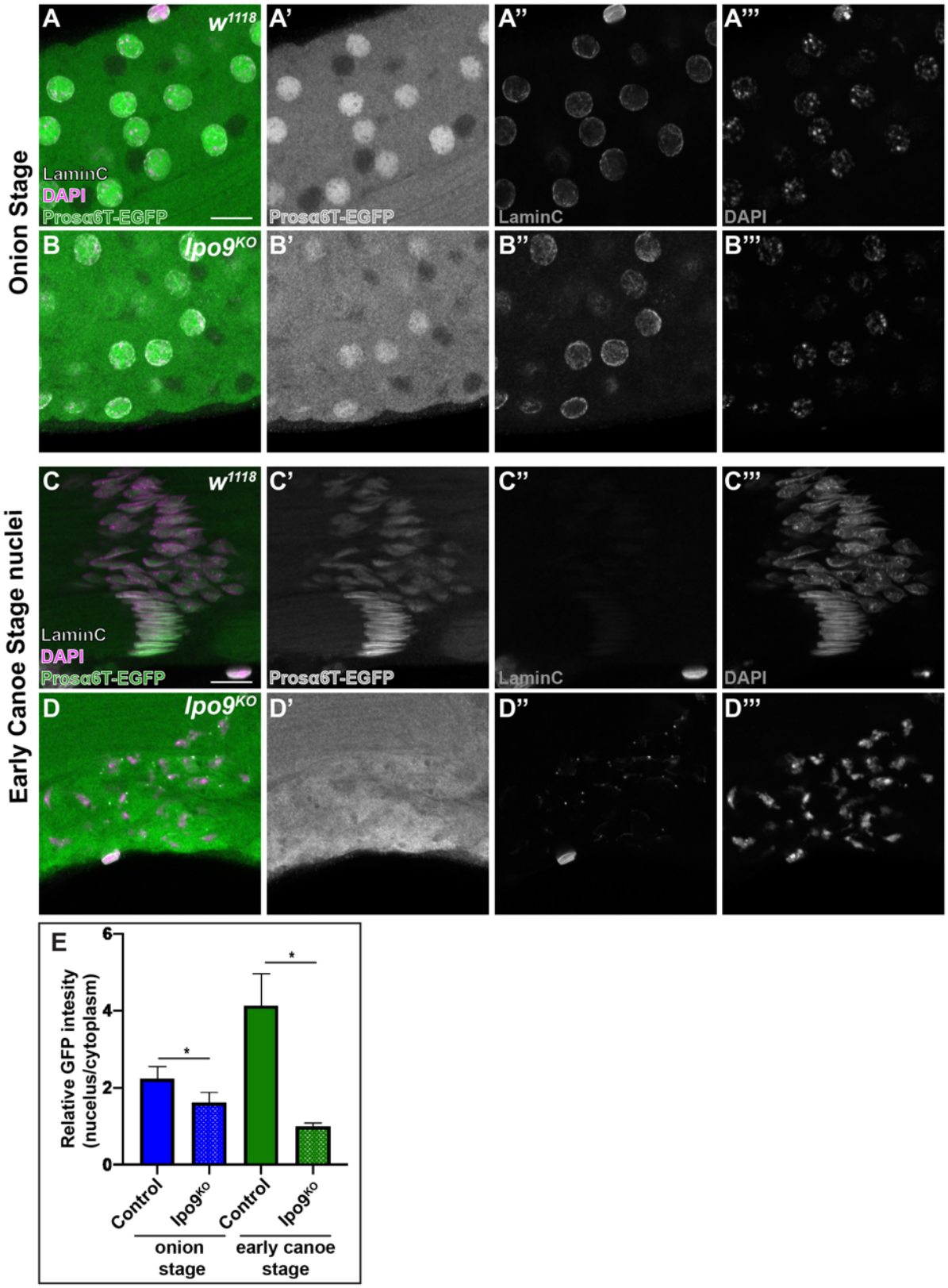

Figure S6. *lpo9*^{KO} spermatids show reduction of Prosα6T in the nucleus. (A-D) Spermatids at the onion stage and early canoe stage, stained for Prosα6T-EGFP (green), LaminC (red) and DNA (blue). (A & C) *w*^{1118} spermatids and (B & D) *lpo9*^{KO} spermatids. E) Quantification of relative

fluorescent intensity of Prosa6T-EGFP in the nuclei and cytoplasm of control and *Ipo9*^{KO} samples n=45 for each genotype at the onion stage and n=40 for each genotype at early canoe stage. Average values and standard deviations are shown on the graph. *P*-values from t-tests are provided as *P ≤0.05, **P≤0.01, ***P≤0.00; NS, non-significant (P>0.05). Scale bars 10µm.

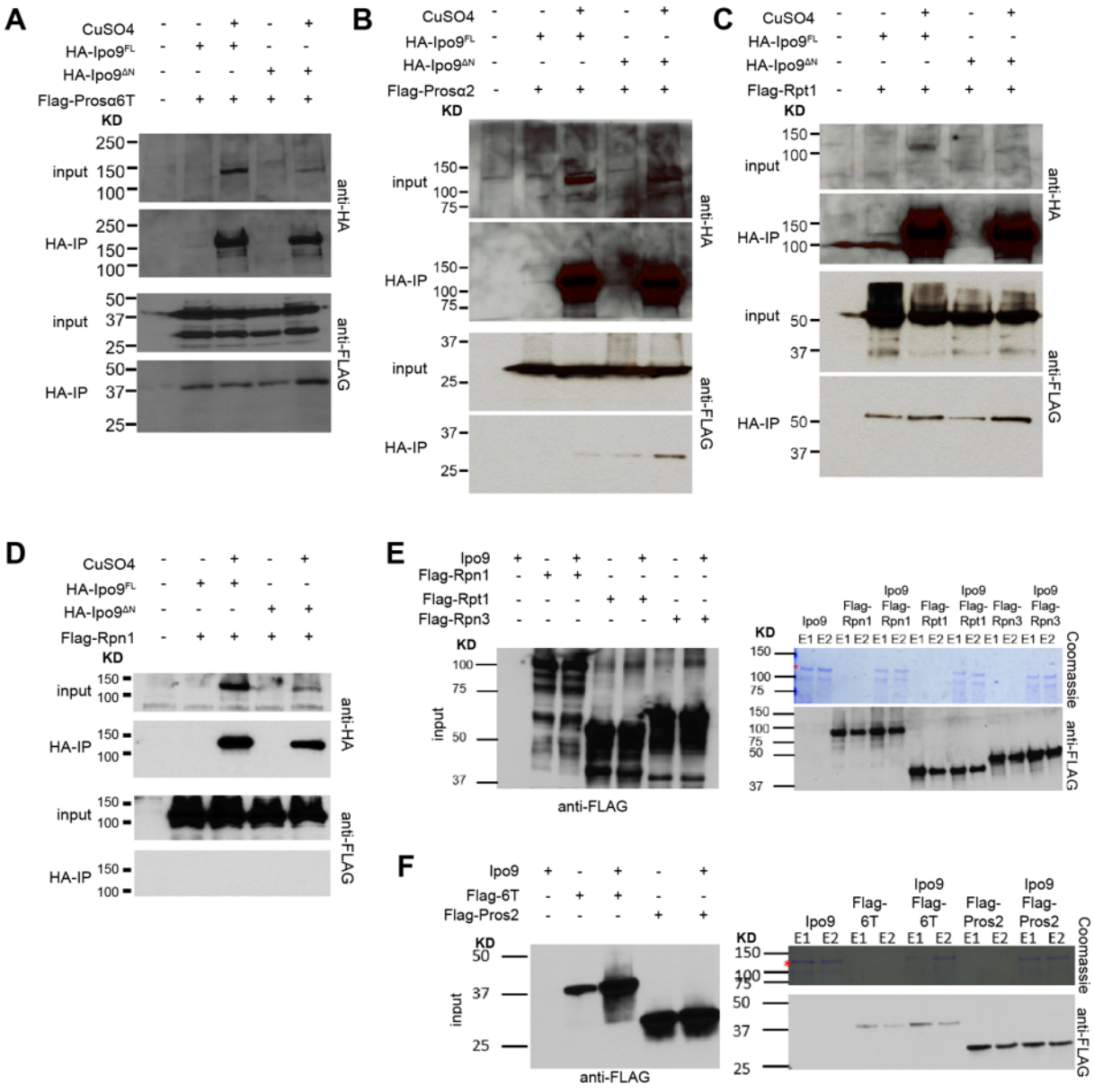

Figure S7. Pulldown binding assays of Ipo9 with proteasomal proteins
(A-D) S2 cells were co-transfected with the indicated DNA encoding HA- Ipo9^{FL} or HA-Ipo9$^{\Delta N}$,FLAG-Prosα6T, FLAG-Prosα2, FLAG-Rpt1 and FLAG-Rpn1. Cell lysates were harvested and subjected to immunoprecipitation with the anti-HA antibody. Western blotting was performed with indicated antibodies. (E-F) In vitro binding assays between Ipo9 and proteasome proteins. (E) Pulldown binding assays of Ipo9 with Rpn1, Rpt1, and Rpn3 (SDS-PAGE/Coomassie Blue and western blot showing FLAG). (F) Pulldown binding assays of Ipo9 with Prosα6T and Prosα2 (SDS-PAGE/Coomassie Blue and western blot showing FLAG).

Table S1: Oligos used in this study

Name	Sequence 5'-3'	Description
Forward Ipo9^{FL}	CACCATGTCGCTGCAATTCCAAAACG	clone Ipo9^{FL} into pENTR
Reverse Ipo9^{FL}	CTACTTCTGCTGGACCTTGCTG	clone Ipo9^{FL} into pENTR
1Forward Ipo9$^{\Delta N}$	CACCATGTCGCTGCAATTCCAAAACG	clone Ipo9$^{\Delta N}$ into pENTR
1Reverse Ipo9$^{\Delta N}$	TTCTGTCTGCTGCAGGACTCC	clone Ipo9$^{\Delta N}$ into pENTR
1.1Reverse Ipo9$^{\Delta N}$	GAGGAGCGTATCTTTGAATTGGGTTCTGTCTGCTGCAGGACTCC	clone Ipo9$^{\Delta N}$ into pENTR
2Forward Ipo9$^{\Delta N}$	CCCAATTCAAAGATACGCTCCTC	clone Ipo9$^{\Delta N}$ into pENTR
2Reverse Ipo9$^{\Delta N}$	CTACTTCTGCTGGACCTTGCTG	clone Ipo9$^{\Delta N}$ into pENTR
Ipo9Aar1outF	CAAGCCGCAAATGATGCTGCTG	PCR1 verification of Ipo9^{KO} allele Molecular Characterization
DsRedstartR	CATGAACTCCTTGATGACGTCCTC	PCR1 verification of Ipo9^{KO} allele Molecular Characterization
DsRedendF	GACTACACCATCGTGGAGCAG	PCR2 verification of Ipo9^{KO} allele Molecular

		Characterization
Ipo9Sap1outR	CTTTGCCTTTGGCTCAGAGAAGC	PCR2 verification of Ipo9^{KO} allele Molecular Characterization
Exon2F	GGAACTGGGTCCAGTAGTCATAC	PCR3 verification of Ipo9^{KO} allele Molecular Characterization
Exon5R	GAGGTGGAGATTCTTGATGCAC	PCR3 verification of Ipo9^{KO} allele Molecular Characterization
arm1F	GCTACACCTGCATGCTCGCGTTCATGTGCAAGCGCAAGTC	To generate Donor plasmid for Ipo9^{KO}
arm1R	GTCACACCTGCACTGCTACAACGGGCGTTTTGCAAGACTG	To generate Donor plasmid for Ipo9^{KO}
Arm2F	CGTAGCTCTTCGTATCAACTTTCTGTCCACCGTTCC	To generate Donor plasmid for Ipo9^{KO}
Arm2R	CGATGCTCTTCCGACGCGAACCGAATCGTAACTGGC	To generate Donor plasmid for Ipo9^{KO}
Guide1	CTTCGCGCTATCACATGTAGTCAA	To create guide RNA

Guide1 complementary	AAACTTGACTACATGTGATAGCGC	To create guide RNA
Guide2	CTTCGGTGGACAGAAAGTTGAGTA	To create guide RNA
Guide2 complementary	AAACTACTCAACTTTCTGTCCACC	To create guide RNA
X chromosome probe	Cy3/TTTTCCAAATTTCGGTCATCAAATAATCAT	
Y chromosome probe	Alexa488N/AATACAATACAATACATTACAATACAATAC	
2nd chromosome probe	Cy5/AACACAACACAACACAACACAACACAACAC	
Prosα6T Forward	CACCATGTTCCGGAATCAGTATGAC	clone Prosα6T into pENTR
Prosα6T Rev	TCAATGTGCGTCACTGCCGC	clone Prosα6T into pENTR
Prosα2 Forward	CACCATGGCTACCGAACGATACAG	clone Prosα2 into pENTR
Prosα2Rev	TTAGGGGATGCTGGCCAAGTAG	clone Prosα2 into pENTR
Rpn1 Forward	CACCATGACGGGCGAGACCAAGCTG	clone Rpn1 into pENTR
Rpn1Rev	CTATTTCACAAAATTTGGGTTCTTTTTCAGTATAACG	clone Rpn1 into pENTR
Rpn3 Forward	CACCATGACCAACGCAACGGACATC	clone Rpn3 into pENTR
Rpn3Rev	TTAGAAACCATCCTCATCATCCTC	clone Rpn3 into pENTR

Rpt1Forward	CACCATGCCGGACTACCTGGGCGAC	clone Rpt1 into pENTR
Rpt1Rev	TTAGTTGTAGGTCATGTAGCGTG	clone Rpt1 into pENTR
pMTIpo9 Forward	tccagtgtggtggaattctgcagatAGCCACCATGGATCTCCACCG CGGTGGA	To clone $Ipo9^{FL}$ and $Ipo9^{\Delta N}$ into pMT
pMTIpo9 Reverse	acagtcgaggctgatcagcgggtttCTACTTCTGCTGGACCTTGCT G	To clone $Ipo9^{FL}$ and $Ipo9^{\Delta N}$ into pMT
Common Forward	GAAGGAGATATACCATGGGCAGCAGCAGCCAAGACTA CAAAGACCATGACGGT	Forward primer for the pAFW vector with extra sequence of VC024 vector
Prosα6TRev VC024	CTTTCTGTTCGACTTAAGCATTATGCTCAATGTGCGTCA CTGCCGC	clone Prosα6T into VC024
Prosα2Rev VC024	CTTTCTGTTCGACTTAAGCATTATGCTTAGGGGATGCTG GCCAAGT	clone Prosα2 into VC024
Rpn1Rev VC024	CTTTCTGTTCGACTTAAGCATTATGCCTATTTCACAAAAT TTGGGTTCTT	clone Rpn1 into VC024
Rpn3Rev VC024	CTTTCTGTTCGACTTAAGCATTATGCTTAGAAACCATCC TCATCATCCTC	clone Rpn3 into VC024
Rpt1Rev VC024	CTTTCTGTTCGACTTAAGCATTATGCTTAGTTGTAGGTC ATGTAGCGT	clone Rpt1 into VC024
Ipo9Forward VC024	GAGGTCTTATTTCAAGGCCCGGGAGGTAGTGGAAGCT CGCTGCAATTCCAAAACGAC	clone Ipo9 into VC024
Ipo9Rev VC024	GGCCCCAAGGGGTTATGCTAGTTATTGCCTACTTCTGC TGGACCTTGCTG	clone Ipo9 into VC024

Table S2: Key Resources

Reagent type (species) or resource	Designation	Source or reference	Identifiers	Additional information
strain, strain background (Escherichia coli)	BL21(DE3)	New England BioLabs	Cat# C2527H	Chemically competent
genetic reagent (*D. melanogaster*)	*Ipo9^{KO}*	This paper	N/A	Fly line maintained in M. Buszczak lab
genetic reagent (*D. melanogaster*)	*UASp-HA-Ipo9^{FL}*	This paper	N/A	Fly line maintained in M. Buszczak lab
genetic reagent (*D. melanogaster*)	*UASp-HA-Ipo9$^{\Delta N}$*	This paper	N/A	Fly line maintained in M. Buszczak lab
genetic reagent (*D. melanogaster*)	*w[1118]; P{w[+mC]=His2Av -mRFP1}III.1 P{w[+mW.hs]=FR T(w[hs])}2A*	Bloomington Drosophila Stock Center	BDSC: 34498; FlyBase; FBti0077846; RRID:BDSC_34498	FlyBase symbol: P{His2Av-mRFP1}III
genetic reagent (*D. melanogaster*)	*y[1] sc[*] v[1] sev[21]; P{y[+t7.7] v[+t1.8]=TRiP.HMS0 0804}attP2* *Ipo9 (*RNAi)	Bloomington Drosophila Stock Center	BDSC: 33004; FlyBase: FBti0140516; RRID:BDSC_33004	FlyBase symbol: P{TRiP.HMS00804}
genetic reagent (*D. melanogaster*)	*w^{1118}*	Bloomington Drosophila Stock Center	BDSC:6326 FlyBase: FBrf0136956; RRID:BDSC_6326	
genetic reagent (*D. melanogaster*)	P{w[+mC]=protamin eB-eGFP}2/CyO; P{w[+mC]=dj-GFP.S}3/TM3, Sb[1]	Bloomington Drosophila Stock Center	BDSC: 58406; FlyBase: FBti0163111; RRID:BDSC_58406	FlyBase symbol: P{protamineB-eGFP}2

genetic reagent (*D. melanogaster*)	*P{w[+mC]=sqh-EYFP-Mito}3*	Bloomington Drosophila Stock Center	BDSC:7194; FlyBase: FBti0038015; RRID:BDSC_7194	FlyBase symbol: P{sqh-EYFP-Mito}3
genetic reagent (*D. melanogaster*)	*P{matalpha4-GAL-VP16}67; P{matalpha4-GAL-VP16}15*	Bloomington Drosophila Stock Center	BDSC: 80361 FlyBase: FBrf0220341; RRID:BDSC_80361	FlyBase symbol: P{matα4-GAL-VP16}
genetic reagent (*D. melanogaster*)	*Prosα6T-EGFP*	(Ma, J. et al 2002)	N/A	
genetic reagent (*D. melanogaster*)	*Prosα3T-EGFP*	(Ma, J. et al 2002)	N/A	
genetic reagent (*D. melanogaster*)	*Prosα2-EGFP*	(Ma, J. et al 2002)	N/A	
genetic reagent (*D. melanogaster*)	*Vasa-gal4*	Gift from Y. Yamashita	N/A	
cell line (D. melanogaster)	S2R+	Drosophila Genomics Resource Center	Cat#150; RRID: CVCL_Z831	
antibody	anti-Vasa (Rat monoclonal)	DSHB	Cat#vasa; RRID:AB_760351	IF (1:20), WB (1:10000)
antibody	anti-1B1 (Mouse monoclonal)	DSHB	Cat#1B1; RRID:AB_528070	IF (1:20)
antibody	anti-Vasa -d-260 (Rabbit polyclonal)	Santa Cruz	Cat# sc-30210; RRID:AB _793874	IF (1:200)

antibody	anti-actin-JLA20 (Mouse monoclonal)	DSHB	Cat#JLA20; RRID:AB_528068	IF (1:10) WB (1:100)
antibody	anti-LaminC-LC28.26 (Mouse monoclonal)	DSHB	Cat#LC28.26; RRID:AB_528339	IF (1:10)
antibody	actin-C4 (Mouse monoclonal)	Millipore Sigma	Cat#MAB1501 RRID:AB_2223041	IF (1:100) WB (1:1000)
antibody	anti-HA (Rat monoclonal)	Roche	Cat#3F10; RRID:AB_2314622	IF (1:100)
antibody	anti-GFP (Rabbit polyclonal)	Invitrogen	Cat#A-11122; RRID:AB_221569	IF (1:1000)
antibody	alpha-Tub [YL1/2] (Rat monoclonal)	Abcam	Cat#Ab6160; RRID:AB_305328	IF (1:100)
antibody	anti-GFP (GFP-1020) (Chicken polyclonal)	Aves Labs	Cat# GFP-1020, RRID:AB_10000240	IF (1:1000)
antibody	anti-Ubiquitin (P4D1) (Mouse monoclonal)	Cell Signalling	Cat#3936 RRID:AB_331292	IF (1:100)
antibody	Rabbit anti-H2A	(Leach et al., 2000)	N/A	IF (1:2000)
antibody	anti-HA (5B1D10) (Mouse monoclonal)	Thermo Fisher	Cat#32-6700 RRID:AB_2533092	WB (1:1000)

antibody	anti-RFP (Rabbit polyclonal)	Rockland	Cat# 600-401-379s RRID:AB_11182807	IF (1:1000)
antibody	Rabbit anti-C(3)G	(Hong et al., 2003)	N/A	IF (1:1000)
antibody	Rabbit anti-C(2)M	(Manheim, E. & McKim, K. 2003)	N/A	IF (1:1000)
antibody	Anti-FLAG M2 (Mouse monoclonal)	Sigma	Cat# F3165, RRID:AB_259529	WB (1:10000)
antibody	anti-Orb (4H8) (Mouse monoclonal)	DSHB	Cat# Orb 4H8; RRID:AB_528418	IF (1:10)
antibody	Anti-Osk Rabbit	Gift from Dr. Ephrussi lab	N/A	IF (1:1000)
recombinant DNA reagent	pAFW (plasmid)	Drosophila Genomics Resource Center	DGRC:1111	
recombinant DNA reagent	pPHW (plasmid)	Drosophila Genomics Resource Center	DGRC: 1101	
recombinant DNA reagent	pMT-puro (plasmid)	Addgene	Cat#17923	
recombinant DNA reagent	VC0024 (plasmid)	Gift from Victor Cruz in Erzberger Lab at UTSW		

recombinant DNA reagent	pU6-BbsI-chiRNA (plasmid)	M. Harrison, K. O'Connor-Giles, J. Wildonger	Addgene Plasmid #45946	
recombinant DNA reagent	pDsRed-attP (Plamid)	M. Harrison, K. O'Connor-Giles, J. Wildonger	Addgene #51019	
commercial assay or kit	pENTR/D-TOPO Cloning Kit	Invitrogen	Cat#K240020	
commercial assay or kit	Gateway LR clonase	Invitrogen	Cat#11791019	
commercial assay or kit	Qiagen Plasmid Midi Kit	Qiagen	Cat#12143	
commercial assay or kit	QIAprep Spin Miniprep kit	Qiagen	Cat#27106	
commercial assay or kit	Anti-HA Affinity Matrix	Roche	Cat# 11815016001	
commercial assay or kit	Effectene Transfection Reagent	Qiagen	Cat#301425	
commercial assay or kit	NI-NTA agarose	Qiagen	Cat#30210	
commercial assay or kit	One-Step Blue Protein Gel Stain	Biotium	Cat#21003-1L	
chemical compound, drug	Rhodamine phalloidin	Invitrogen	Cat# R415 300U	

chemical compound, drug	4′,6-Diamidino-2-phenylindole dihydrochloride (DAPI)	Sigma-Aldrich	Cat#CD9542	
chemical compound, drug	Protease inhibitor	Roche	Cat#11836170001	
chemical compound, drug	Paraformadehyde Aqueous Solution - 16% - 10mL	Electron Microscopy Sciences	Cat#27423	
chemical compound, drug	T4 DNA Polymerase	New England Biolabs	Cat#M0203S	
software, algorithm	FIJI (Fiji Is Just ImageJ)	NIH	https://imagej.net/Fiji/Downloads	
software, algorithm	Prism 9	GraphPad	N/A	
software, algorithm	Flycrispr design tool		http://flycrispr.molbio.wisc.edu/tools	
software, algorithm	Proteome Discoverer 2.2		N/A	

Table S3: Proteins associated with Importin-9
Protein samples from the Importin-9 immunoprecipitation were sent to the Proteomics Core Facility at UT Southwestern. The data were analyzed using Proteome Discoverer 2.2 and was searched using the Drosophila melanogaster protein database from Uniprot.

Click here to Download Table S3